Original paper

A geological, geochemical and textural study of a LCT pegmatite: implications for the magmatic versus metasomatic origin of Nb–Ta mineralization in the Moose II pegmatite, Northwest Territories, Canada

Melissa O. ANDERSON[1]*, David R. LENTZ[1], Chris R. M. MCFARLANE[1], Hendrik FALCK[2]

[1] *Department of Earth Sciences, University of New Brunswick, PO Box 4400, 2 Bailey Drive, Fredericton, New Brunswick, E3B 5A3, Canada; anderson.geology@gmail.com*

[2] *Northwest Territories Geoscience Office, PO Box 1500, 4601-B 52 Avenue, Yellowknife, Northwest Territories, X1A 2R3, Canada*

* *Corresponding author*

The internal zonation and chemical evolution of Nb–Ta oxides and muscovite have been characterized in the Moose II pegmatite, Northwest Territories, Canada, to distinguish primary magmatic mineralization from that formed during late-stage metasomatic processes. In addition, muscovite associated with Nb–Ta oxides was examined in order to assess the evolution of the pegmatite melt and the nature of the late-stage fluids.

Detailed mapping shows that the studied body (430 × 61 m) is a highly fractionated, irregularly zoned, spodumene-subtype rare-element pegmatite dominated by coarse-grained to megacrystic albite, K-feldspar, and spodumene, with intergranular assemblages of quartz, K-feldspar, albite, spodumene, muscovite, and minor amblygonite–montebrasite. Monomineralic core zones (quartz and amblygonite–montebrasite), aplitic albite 'pods,' and units characterized by phyllic alteration occur in the central portions of the pegmatite.

Columbite–tantalite minerals occur throughout the pegmatite, excluding the quartz cores, and patterns of internal zoning include: (1) normally zoned ferrocolumbite with early Ta–Ti-rich, and later Nb–W-rich overgrowths; (2) oscillatory zoned Ti-rich ferrotantalite with Nb-rich patchy replacement; (3) reversely zoned ferrocolumbite, with Ta-rich cores and (4) complexly zoned Ti-rich ferrotantalite with abundant late Nb- and Ta-rich patches and sieve textures.

The textures and chemical patterns demonstrate an evolution from columbite to tantalite, whereby the Ta/(Ta + Nb) ratio increased with progressive fractionation (0.13–0.59) but the Mn/(Mn + Fe) ratio remained nearly constant (0.15–0.31). The chemical evolution of the Nb- Ta oxides from columbite to tantalite is consistent with crystallization from a magmatic to late-stage magmatic Na-rich melt, with a sequence of crystallization progressing from those of the wall zone, to the first intermediate zone, and finally the late aplitic albite zones. Minor remobilization of Nb, and to a lesser extent Ta, was responsible for some of the replacement features found in the Nb–Ta oxides. Textural observations and trace-element analyses of fine-grained, secondary muscovite found throughout the pegmatite indicate hydrothermal metasomatism by a late F- and Nb-rich vapor-like "supercritical" fluid.

Keywords: Moose II pegmatite, columbite–tantalite, Nb–Ta chemical evolution, muscovite trace-element geochemistry, Yellowknife pegmatite field, Northwest Territories

Received: 14 March 2013; accepted: 2 October 2013; handling editor: P. Uher

The online version of this article (doi: 10.3190/jgeosci.149) contains supplementary electronic material.

1. Introduction

Pegmatites represent highly evolved granitic melts that are the result of protracted fractional crystallization (London 2008) and are of scientific interest as they display complex and diverse mineralogy, textures, structures, and petrogenetic relationships, with evolved geochemical signatures, which have challenged petrologists in terms of the origin and processes of formation.

The principal ore minerals of Nb and Ta in rare-element pegmatites are oxides, in particular the columbite–tantalite minerals [$(Fe,Mn)(Ta,Nb)_2O_6$]. Many workers have examined these phases in terms of their crystal chemistry and zonation (e.g., Tindle and Breaks 2000; Novák et al. 2003; Chudík et al. 2011), relationship with other Nb–Ta minerals (e.g., Černý et al. 1986; Van Lichtervelde et al. 2007), and mineral structures (e.g., Ercit et al. 1995). Recently, experimental studies have investigated the solubility of columbite–tantalite in granitic melts and aqueous fluids (Linnen and Keppler 1997; Linnen 1998; Chevychelov et al. 1998, 2004, 2005, 2010; Zaraisky et al. 2010).

It is well established that columbite–tantalite is initially concentrated in pegmatites by processes active during protracted (extreme) fractional crystallization of granitic melts (Černý et al. 1986; London 2008). Subsequent stages of enrichment may be driven by later magmatic- or hydrothermal–metasomatic processes (Linnen et al.

2012). Despite the large amount of literature on these important mineral species, the processes that control the distribution and grade of Nb–Ta mineralization in pegmatites remain poorly constrained. This contribution examines (1) the styles of Nb–Ta mineralization and their chemical evolution, and (2) the major- and trace-element chemistry of muscovite to assess and constrain the processes of formation (i.e., magmatic *versus* metasomatic) in evolved rare metal pegmatites using the Moose II pegmatite (Yellowknife pegmatite field, Northwest Territories, Canada) as a case study.

2. Geological setting

The study area is located in the southern part of the Archean Slave Craton, Northwest Territories, Canada, approximately 115 km east–southeast of Yellowknife, NT (Fig. 1). The focus of this study, the Moose II pegmatite, is part of an extensive pegmatite swarm, the Yellowknife pegmatite field, located in supracrustal rocks of the Yellowknife Basin between the Yellowknife Volcanic Belt and the Eastern Batholith (Meintzer 1987). The geological and metallogenic evolution of the Slave Craton was summarized by Bleeker and Hall (2007), expanding on earlier work by authors such as Henderson (1981), Ayres and Černý (1982), Padgham and Fyson (1992), King and Helmstaedt (1997), and Bleeker and Davis (1999). The regional geological setting was described in detail by Anderson (2013).

The host rock for the Moose II pegmatite is the Yellowknife Supergroup supracrustal assemblage, in particular, the metamorphosed greywacke–mudstone turbiditic rocks of the Burwash Fm., deposited in the Archean Burwash Basin – a large basin that is up to120 km wide and at least 180 km long. The sedimentary rocks were derived from contemporaneous volcanic and granitic rocks whose source remains unknown (Henderson 1987).

3. Geology of the Moose II pegmatite

3.1. Mode of occurrence and structural features

The Moose II pegmatite is a north-trending dike, 427 m long by 61 m wide, exposed as three segments – the north, central, and south sections (Fig. 2). The south and central sections are considered to be one offset dike; however, the continuity between the central and north sections at depth is unknown and they likely represent individual dikes. In subsequent discussions, all three of the sections will be referred to as one pegmatite. The dike(s) dip between 50º and 80º to the west with the steepest dips in the north. The strike of the pegmatite is oblique to the primary bedding of the Burwash Fm. metasedimentary rocks, which trend ~060°/70°S. The contacts with the host rock are sharp, locally well exposed (Fig. 3). Shearing at the contacts is common, as defined by a strong sub-vertical cleavage and alignment of phyllosilicate minerals in a zone up to 1 m in width. A late phase of brittle deformation post-dated pegmatite consolidation, as demonstrated by the sinistral strike-slip fault that offsets the central and south sections of the pegmatite (Fig. 2).

The Moose II pegmatite melt was likely injected into part of a dilatant zone in a related north-trending fault system, as indicated by the orientation of the pegmatite dikes, and its proximity to the north-trending craton-wide Beaulieu River Fault Zone (BRFZ), located approximately 2.5 km to the east of the pegmatite bodies (Bleeker et al. 1999; Fig. 1). The size and complexity of the pegmatite suggest multiple extensional events with successive pulses of magma injections. The distribution and orientation of the pegmatite bodies are consistent with a sinistral shear zone-related mechanism of emplacement (Fig. 4).

3.2. Age of the Moose II pegmatite

The crystallization age of the Moose II pegmatite was determined by U–Pb dating of primary euhedral ferrocolumbite (LA ICP-MS; Anderson 2013) at 2562 ± 15 Ma (MSWD = 0.45). This age is, as expected, younger than the depositional age for the Burwash Fm. metasedimentary host rocks, dated at 2661 ± 2 Ma (U–Pb zircon crystallization age of interbedded felsic tuff, Ootes et al. 2009). More importantly, it is close to the age of the nearest fertile peraluminous granites, known as Prosperous Suite plutons. This suite of granites is located approximately 70 km to the northwest (Fig. 1) of the study area and two of these plutons have been dated at 2602 ± 2 Ma and 2596 ± 2 Ma (U–Pb monazite, Davis and Bleeker 1999). Thus, as with other settings, age constraints for pegmatites do not overlap the time for regional felsic magmatism. The crystallization age of the Moose II Pegmatite corresponds to a period of late magmatism in the Slave Craton during which few other tectonic or magmatic events are recorded.

3.3. Mineralogical zonation of the Moose II pegmatite

The Moose II pegmatite displays an irregular, yet simple, zonation of mineralogical assemblages, as shown in Fig. 2, and outlined in Tab. 1.

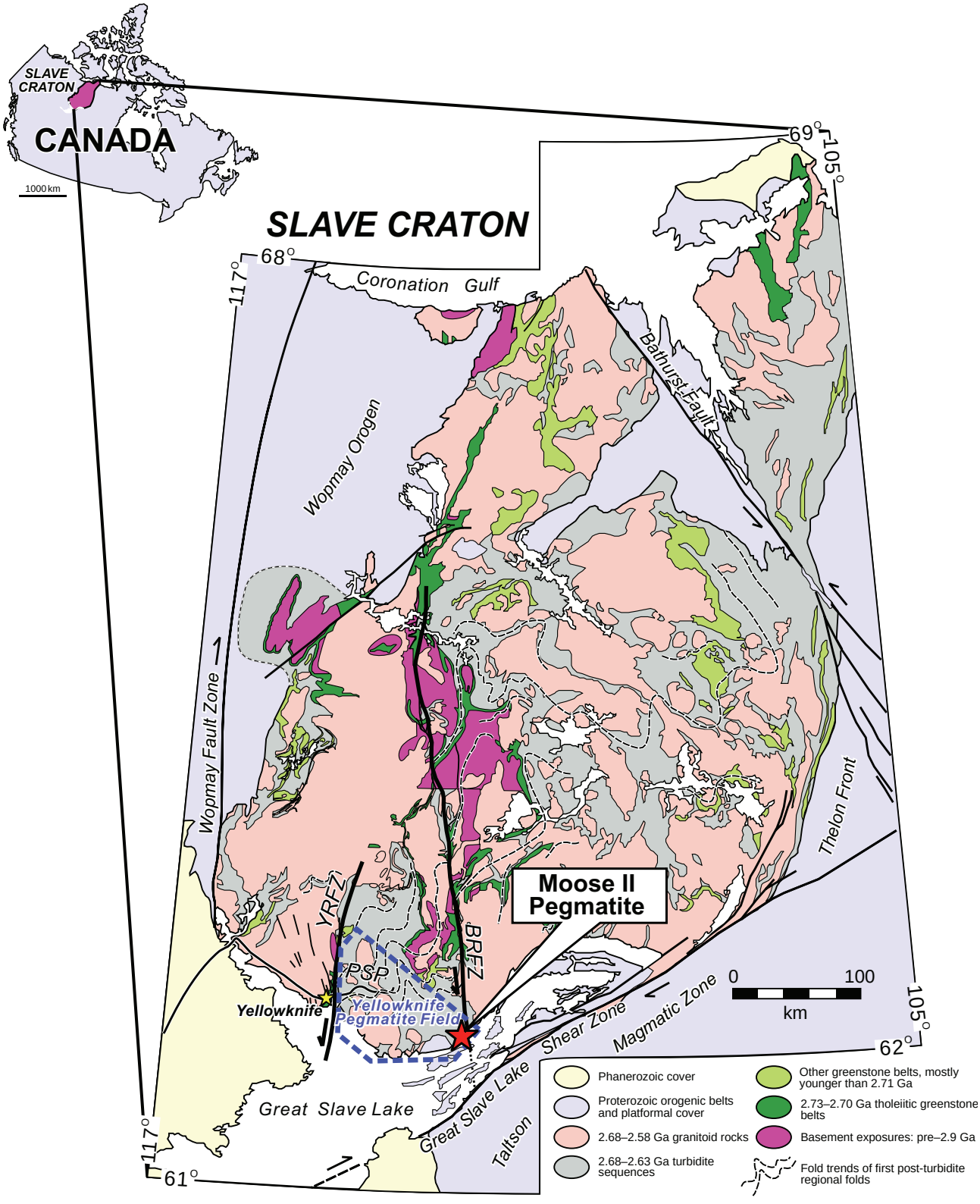

Fig. 1 Geological map of the Slave Craton after Bleeker and Hall (2007). The location of the Moose II pegmatite and the approximate extent of the Yellowknife (YK) pegmatite field, outlined by the dashed blue line, are also shown. YRFZ = Yellowknife River Fault Zone, BRFZ = Beaulieu River Fault Zone, PSP = Prosperous Suite Plutons.

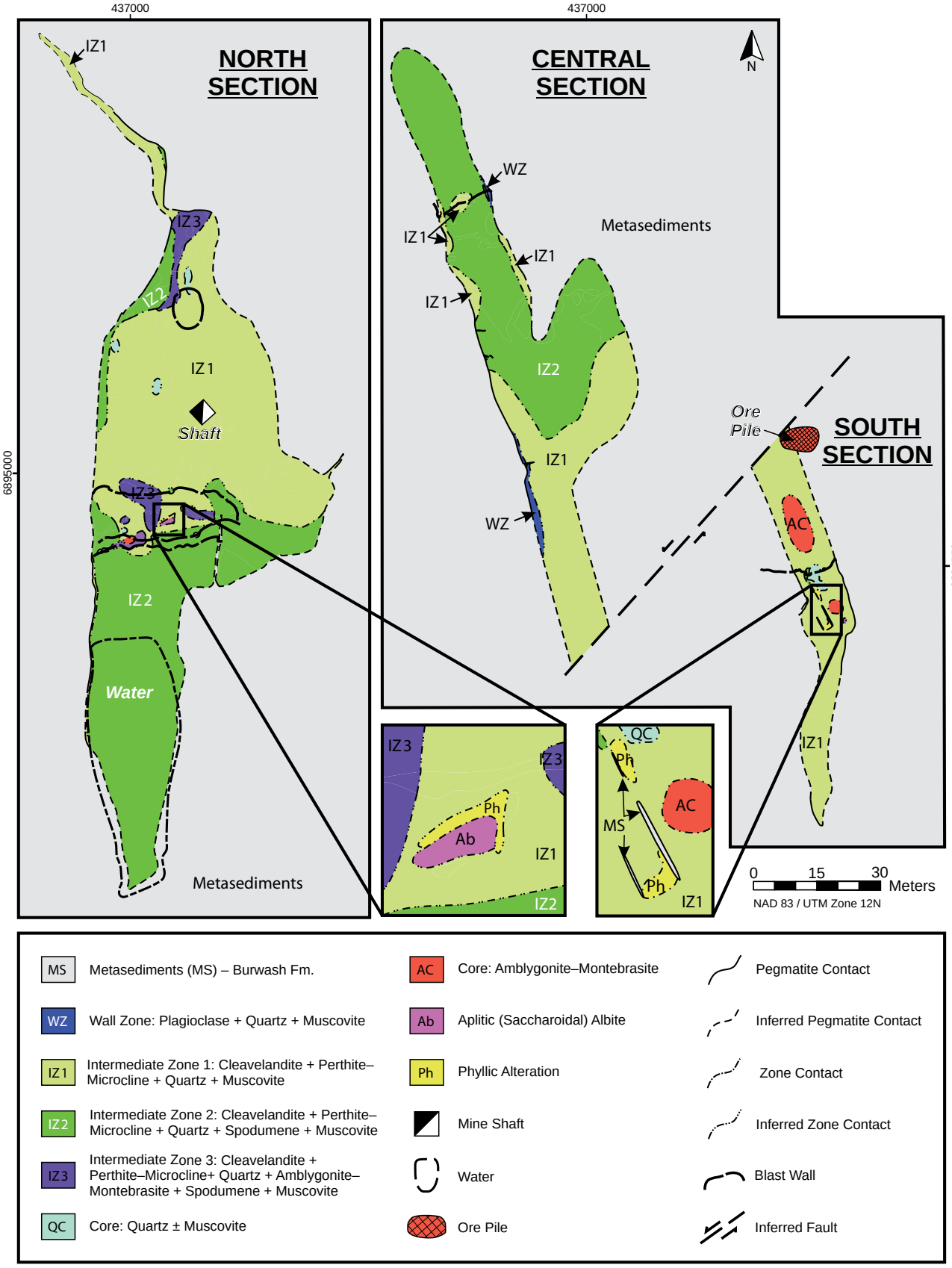

Fig. 2 Simplified geological map of the Moose II rare-metal pegmatite, showing the different mineralogical zones. Datum: NAD83, UTM Zone 12N.

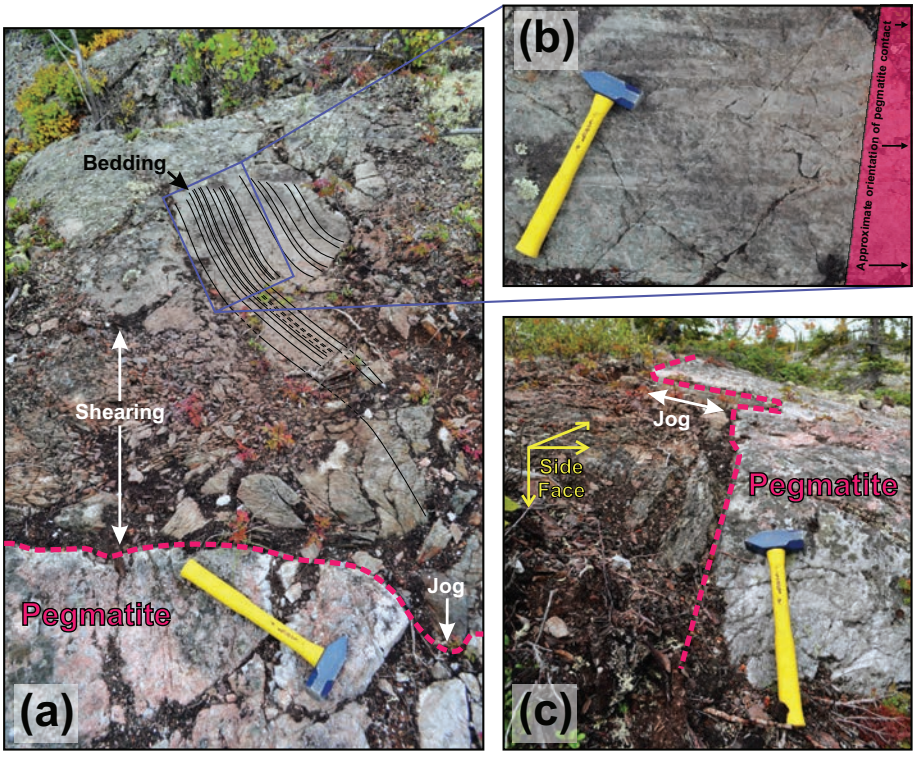

Fig. 3 Photographs of the contact between Burwash Fm. metaturbidite rocks and the Moose II pegmatite, central section, western contact: **a –** Bedding planes (traced) are oriented oblique to the pegmatite–host rock contact and shearing of the host rock and jog in the contact are indicated; photo facing west; **b –** Close up of the bedding preserved by nodular cordierite, photo facing north; **c –** Side view of the pegmatite–host rock contact which is steeply dipping to the west; note that a jog in the contact is indicated; photo facing north. Hammer shaft length is 35.56 cm.

Grain-size variability is extreme, ranging from aplitic (sub-mm scale) to megacrystic (≤ 1 m crystals). Anisotropic growth textures of spodumene and feldspars are common at margins where the long axes of crystals are perpendicular to the pegmatite–wall rock contact. The pegmatite bodies are dominated by coarse-grained to megacrystic albite, K-feldspar, and spodumene and intergranular assemblages of quartz, K-feldspar, albite, spodumene, muscovite, and minor amblygonite–montebrasite. Monomineralic core zones (quartz and amblygonite–montebrasite), aplitic albite 'pods', and late phyllic alteration (muscovite-rich replacement) units are also observed in the central portions of the pegmatite. Primary blocky K-feldspar has undergone extensive sodic metasomatism which resulted in an abundance of pink bladed albite (cleavelandite). Intergranular aplitic albite is abundant in the north section of the pegmatite.

If not specified otherwise, all mineral abbreviations used in the text are after Whitney and Evans (2010).

3.4. Phyllic alteration

Phyllic alteration affects the intermediate zones of the Moose II pegmatite in both the north and south sections, resulting in 10–90% replacement of primary feldspars by muscovite + quartz. This replacement unit is associated with an aplitic albite zone in the north section, and in the south section with the wallrock xenoliths aligned parallel to the pegmatite–wallrock contacts (Fig. 2). Textural evidence for replacement includes the occurrence of pseudomorphs of muscovite after feldspars.

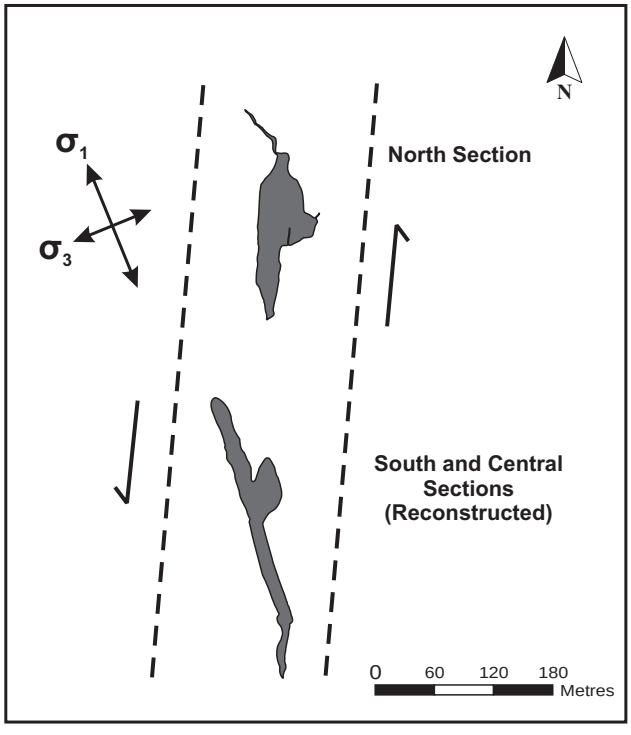

Fig. 4 Structural model for emplacement of the moderately to steeply dipping Moose II pegmatite(s) into a sinistral shear zone. South and central sections reconstructed from the late E–W faulting. σ_1 is the maximum and σ_3 the minimum principle stress orientation.

Tab. 1 Summary of the mineralogical zones in the Moose II pegmatite

Zone	Distribution	Contacts	Grain Size	Primary Mineralogy	Intergranular Assemblage	Accessory Minerals	Textures
Border Zone	1–8 cm selvage around entire pegmatite	Gradational	Fine-grained (< 0.5 cm)	Qz + Pl ± Ms		Tur, Clf–Tnf	Comb-textured Tur
Wall Zone	Asymmetrical distribution, few cm to 2 m wide	Gradational	Coarse-grained (< 5 cm)	Qz + Pl ± Ms		Tur, Clf–Tnf	Comb-textured feldspars
Intermediate Zone 1	All sections	Gradational	Medium- to coarse-grained (< 30 cm)	Clv + Kfs + Qz + Ms	Clv + Ksp + Qz	Clf–Tnf, Rt, Ap (F), Brl, Cal, Sph, Zrn, Py, Urn	Local comb-texture, plumose Clv
Intermediate Zone 2	Central and north sections	Gradational	Medium- to very coarse-grained (< 1 m)	Clv + Kfs + Spd + Ms	Qz + Ab + Kfs + Spd + Ms	Clf–Tnf, Brl, Cst, Rt, Ap (F), Zrn, Gr, Sph, Py, Cpy	Comb-textured Spd
Intermediate Zone 3	North Section	Gradational	Aplitic to coarse-grained (< 20 cm)	Qz + Pl ± Ms	Qz + Ab + Kfs + Ms	Clf–Tnf, Cran (after Amb–Mbr), Ap (F), Cst, Rt, Lzl, Zrn, Py, Gr	Skeletal Amb-Mbr
Quartz Core Zone	South and north sections	Sharp	Fine- to medium-grained (< 5 cm)	Qz ± Ms		Clf–Tnf	"Pods"
Amblygonite–Montebrasite Core Zone	South and north sections	Sharp	Fine- to medium-grained (< 5 cm)	Amb–Mbr		Clf–Tnf, Gr	"Pods"
Aplitic Albite Zones	South and north sections	Sharp	Very fine-grained (aplitic)	Ab		Clf–Tnf, Cst, Tpz, Ap (F), Rt	Minor secondary Qz veins

4. Sampling and analytical methods

4.1. Whole-rock geochemistry

Five bulk samples (> 5 kg) come from the wall zone and each of the intermediate zones. Two chip samples were collected from the aplitic albite and phyllic alteration zones along 2 m intervals, maintaining a consistent width and depth of ~3 cm. Finally, 42 channel samples were obtained using a rock saw and chisel, ~5 cm wide by 5 cm deep, along intervals of one metre.

Samples were analysed by Acme Laboratories in Vancouver, Canada. Major-element analyses by ICP-AES followed a lithium borate fusion and acid dissolution (method ME–MS81). Analyses by ICP-MS were employed for rare-earth and other trace elements (method ME–ICP06), including lithium (method Li–OG63), using a specialized four-acid digestion technique. This procedure involved heating of a 0.25 g split in HNO_3 – $HClO_4$ – HF to fuming until dry. The remaining residue was dissolved in HCl and subsequently analyzed by ICP-MS. Additional sampling and analytical details are available in Anderson (2013).

4.2. Nb–Ta oxide analyses

Representative samples from all zones were studied petrographically to determine mineral associations. Subsequent backscattered electron (BSE) imaging was done using a JEOL JSM6400 Digital scanning electron microscope (SEM) equipped with Geller dPict digital image acquisition software at the University of New Brunswick Microscopy and Microanalysis Facility (UNB-MMF). A total of 78 spot analyses were performed on the Nb–Ta oxides done using a JEOL JXA-733 electron probe micro-analyzer (EPMA) equipped with four 2-crystal wavelength-dispersive spectrometers, a Geller Microanalytical automation control, a PGT Prism 2000 energy dispersive spectrometer, and a PGT Spirit X-ray analysis system, at UNB-MMF. A 15 keV accelerating potential and a 200 nA probe (cup) current were used for the analyses. Standards used were: olivine (MgK_α), clinopyroxene (CaK_α), SrTiO3 (TiK_α), bustamite (MnK_α), iron metal (FeK_α), yttrium aluminate (YL_α), zircon (ZrL_α), Nb, Sn, Sb, and Ta metals (NbL_α, SnL_α, SbL_α, and TaL_α), $CaWO_4$ (WM_α), crocoite (PbM_α), and Th and U metals (ThM_α and UM_α). Structural formulae were calculated using 6 O and the software of Tindle (2001a).

4.3. Muscovite analyses

Muscovite from the wall zone, all of the intermediate zones, and the phyllic alteration zone (south section) was characterized petrographically to distinguish different generations (i.e., primary *versus* secondary). In order

to determine the major-element composition, a total of 93 EPMA analyses were performed at UNB-MMF, as described above. Standards used were: clinopyroxene (NaK_α, SiK_α, CaK_α), olivine (MgK_α), plagioclase (AlK$_\alpha$), orthoclase (KK_α), SrTiO3 (TiK_α), bustamite (MnK_α), iron metal (FeK_α), pollucite (CsL_α), barite (BaL_α), Campolingo tremolite (FK_α), and tugtupite (ClK_α).

In situ concentrations of trace elements on the same muscovite samples were determined using a Resonetics M-50-LR 193 nm Excimer laser-ablation system coupled to an Agilent 7700x quadrupole ICP-MS at UNB; a total of 88 analyses were obtained. The concentration of Al_2O_3 previously determined by EPMA was employed for internal standardization. The NIST 612 glass was used as the primary external reference material, and the T1-G MPI-DING glass as a quality control standard. The laser conditions were as follows: laser spot size = 64 μm, fluence = 2 J/cm^2, scan speed = 10 μm/s, repetition rate = 10 Hz. The ablated material was transported out of the cell in a 750 ml/min He cell gas and combined downstream with Ar (750 ml/min) and N_2 (2.8 ml/min) carrier gas prior to entering the ICP-MS torch. Structural formulae were calculated using 24 (O, OH, F) and the software of Tindle (2001b).

5. Whole-rock geochemistry

The average results of the whole-rock geochemistry for individual zones of the studied pegmatite are shown in Tab. 2, and were discussed in detail by Anderson (2013). The trace-element compositions within each of the zones are highly variable; however, several important features are observed. The samples are generally depleted in transition and base metals (Ag, Co, Cr, Cu, Ni, Mo, Pb, and Zn) and REE, with a moderate enrichment of Zn (up to 120 ppm) and Sn (up to 470 ppm) relative to average crustal abundances (Wedepohl 1995). There is also enrichment in the alkalis and alkaline earth elements, up to 1520 ppm Rb, 608 ppm Sr, 257 ppm Ba, 67 ppm Ga, and 63 ppm Cs. Lithium concentrations are highly variable, ranging from < 0.017 to 2.73 wt. % Li_2O (avg. 0.44 wt. % Li_2O), with the highest values in the second intermediate (spodumene-rich) zone. The highest values of Nb and Ta are found in the phyllic alteration zones with up to 1520 ppm Nb and 770 ppm Ta.

6. Niobium–tantalum oxide internal zonation patterns

6.1. Petrography

Niobium–tantalum oxides are found throughout the pegmatite, including the wall zone, intermediate zones, amblygonite–montebrasite core zones, aplitic (saccharoidal) albite zones, and areas of phyllic alteration. In the wall and intermediate zones, the Nb–Ta oxides occur as fine- to medium-grained (< 2 cm) tabular, blocky, or platey crystals, euhedral to subhedral in shape, and disseminated to intergrown with the primary rock-forming minerals, including quartz + cleavelandite + microcline perthite + muscovite ± spodumene ± amblygonite–montebrasite. The amblygonite–montebrasite core zones contain intergranular, medium- to coarse-grained euhedral Nb–Ta oxides. In the aplitic albite zones, the Nb–Ta oxides are very fine-grained, subhedral to euhedral, and disseminated. The phyllic alteration units contain fine-grained (< 5 mm), anhedral Nb–Ta oxides, with sieve and skeletal or corroded textures. Rare inclusions of Nb–Ta oxides occur in fine-grained secondary muscovite throughout the pegmatite. In general, the Nb–Ta oxides are found intimately associated with muscovite of variable grain sizes (up to a few cm across).

6.2. Patterns of internal zonation

As seen in the BSE images, zoning patterns in the columbite–tantalite phases range from simple to complex due to Nb–Ta and Fe–Mn substitutions. The following patterns of internal zonation are identified based on chemical and textural features:

6.2.1. Normal zoning

Normal zoning refers to columbite or tantalite crystals with relatively homogenous cores, which follow normal fractionation patterns of decreasing Nb/Ta from the core to the rim of the primary crystals (Fig. 5a–b; Černý and Ercit 1985). This internal zoning pattern is the most common and occurs in all the zones of the Moose II pegmatite.

6.2.2. Oscillatory zoning

Oscillatory zoning is characterized by episodic variations of Nb- and Ta-rich zones (Fig. 5c–d). The crystal zones are regular, narrow, and often truncated by other zones. Such internal zonation patterns are found primarily in the saccharoidal albite zone, and also occur in the second intermediate zone and the amblygonite–montebrasite core zone. Oscillatory zoning is common in columbite–tantalite and wodginite in many of the large tantalum deposits worldwide (e.g., Černý et al. 1992; Tindle and Breaks 2000; Van Lichtervelde et al. 2007).

6.2.3. Reverse zoning

Reverse zoning consists of a Ta-rich core, becoming Nb-rich towards the rim (Fig. 5e–f). The rimward increase

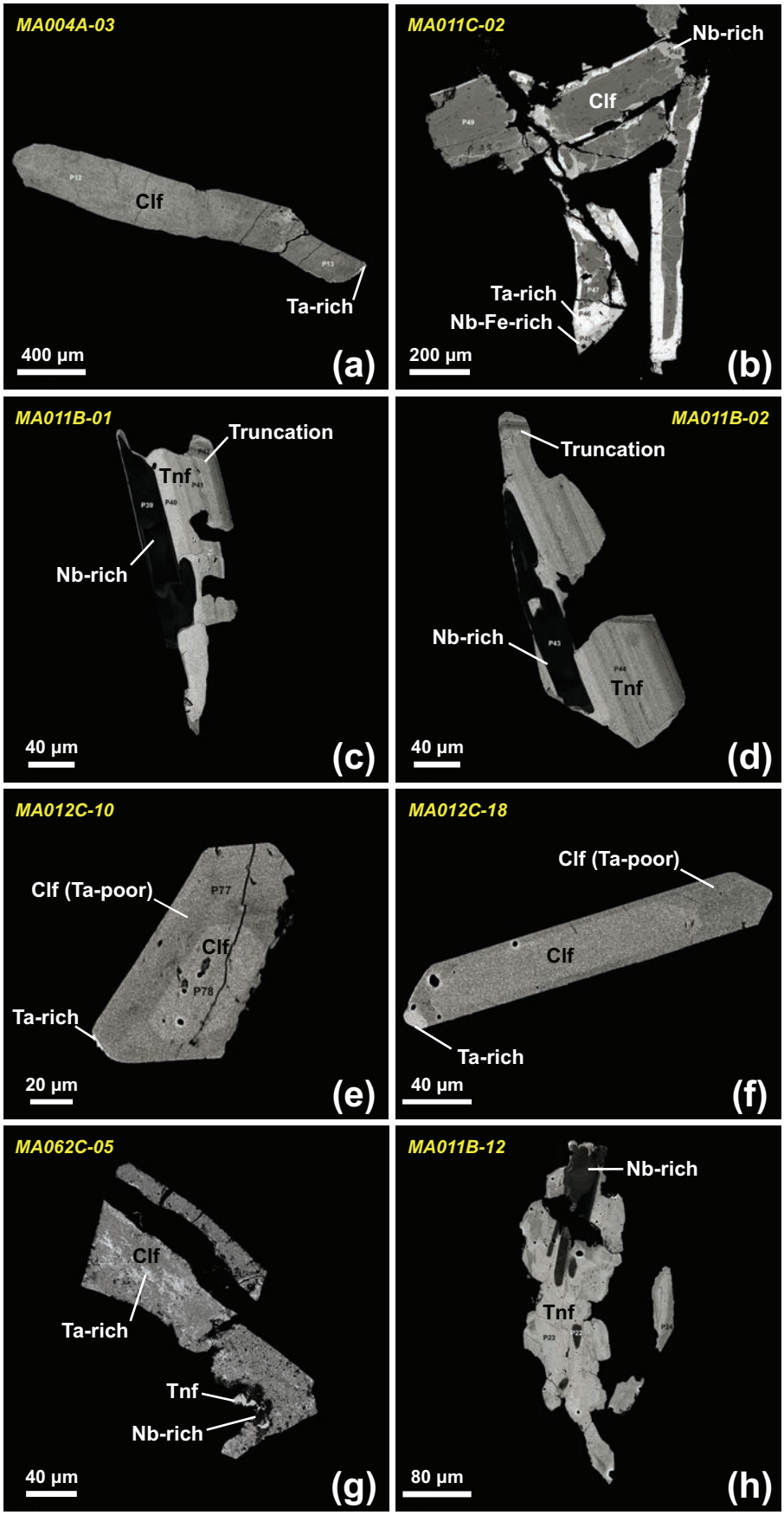

in the Nb/Ta ratio is opposite to expected fractionation patterns; hence the designation of reverse crystal zoning (Lahti 1987). The reverse zoning is rare, and weakly developed; it is only identified in the wall zone of the Moose II pegmatite.

6.2.4. Complex zoning

Complex zoning occurs in subhedral to anhedral columbite–tantalite crystals, showing Nb-rich patchy replacement, sieve and skeletal textures, and local inclusions of uraninite (Fig.5g–h). Fine-grained secondary mica fills sponge-like holes in the crystals. The sequence of replacement (Ta- or Nb-rich) is typically difficult to decipher. This zonation style occurs primarily in areas of phyllic alteration, and to a lesser extent in the wall zone and the aplitic albite zone.

Fig. 5 Back-scattered electron images of various modes of zoning in the columbite–tantalite crystals. *Normal zoning:* **a –** Unzoned ferrocolumbite (Clf) crystal core (medium grey) with a thin Ta-rich overgrowth (bright grey); **b –** Ferrocolumbite core (dark grey) with multiple generations of overgrowths; Ta-rich overgrowths (bright grey) replace primary ferrocolumbite crystals, and later Nb–Fe-rich and Nb--rich overgrowths (medium grey) replace both primary crystals and Ta-rich overgrowths. Late fracture-fills cross cut the crystals; *Oscillatory zoning of ferrotantalite (Tnf), with regular oscillations between Nb- and Ta-rich compositions:* **c–d –** Early oscillations are truncated by later ones, as indicated. Patchy replacement is Nb-rich and irregularly zoned. *Reverse zoning of ferrocolumbite*. **e–f –**The core is enriched in Ta relative to the rims, contrary to normal fractionation patterns. Ta-rich overgrowths are common. *Complex zoning*: **g –** Ferrocolumbite with Ta-rich replacement along microfractures (composition altering to ferrotantalite) and Nb-rich patchy replacement. Sieve texture throughout; **h –** Anhedral ferrotantalite with patchy zonation and Nb-rich replacement. Minor sieve texture.

Tab. 2 Average chip, channel, and bulk analyses by ICP-MS and ICP-AES for each of the mineralogical zones, calculated using half below detection limit (bdl) values when necessary.

	Wall	IZ 1	IZ 2	IZ 3	Ab	Phy
SiO_2 – wt.%	69.70	70.18	70.98	67.89	67.17	65.90
TiO_2	0.01	0.01	0.01	0.015	0.01	0.02
Al_2O_3	16.10	16.26	15.74	15.87	18.03	20.90
Fe_2O_3	0.38	0.62	0.90	0.55	0.26	0.41
CaO	0.59	0.79	1.08	1.47	0.64	0.24
MgO	0.05	0.09	0.15	0.08	0.03	0.03
Na_2O	7.26	6.46	4.20	5.04	9.67	2.05
K_2O	1.12	1.45	2.01	1.79	0.51	4.77
MnO	0.01	0.02	0.04	0.01	0.01	0.02
P_2O_5	0.50	0.88	1.42	3.78	0.63	0.21
Li_2O	*bdl*	0.119	0.781	0.572	0.039	0.032
L.O.I.	1.20	1.75	1.75	1.82	0.90	3.68
Total	96.90	98.51	98.31	98.33	97.83	98.20
Ag – ppm	*bdl*	*bdl*	*bdl*	*bdl*	*bdl*	6.00
Ba	38.9	42.9	68.0	59.8	28.2	16.5
Ce	4.0	4.0	4.5	2.9	3.9	1.3
Co	0.6	6.2	5.6	5.4	0.6	*bdl*
Cr	10	10	12	14	13	10
Cs	6.3	21.7	27.0	16.0	3.5	59.7
Cu	11	29	23	21	8	*bdl*
Dy	0.09	0.24	0.26	0.25	0.23	*bdl*
Er	*bdl*	0.10	0.11	0.12	0.09	*bdl*
Eu	0.08	0.19	0.40	0.29	0.27	*bdl*
Ga	19.1	25.1	27.3	21.7	25.8	66.7
Gd	0.23	0.34	0.53	0.40	0.45	0.08
Hf	0.9	2.4	1.4	0.9	5.1	1.9
Ho	0.03	0.03	0.04	0.03	0.03	*bdl*
La	2.3	3.3	3.5	2.3	2.9	1.0
Lu	*bdl*	0.02	0.01	0.02	0.02	*bdl*
Mo	*bdl*	*bdl*	*bdl*	*bdl*	*bdl*	*bdl*
Nb	59.7	132.3	110.5	79.7	201.7	1520.0
Nd	1.7	1.7	1.9	1.5	1.8	0.5
Ni	*bdl*	5	7	*bdl*	*bdl*	*bdl*
Pb	13	8	8	8	8	6
Pr	0.40	0.42	0.50	0.32	0.41	0.08
Rb	212	436	511	400	37	1875
Sm	0.26	0.34	0.40	0.35	0.40	0.09
Sn	148.0	78.5	85.6	94.5	44.3	392.0
Sr	94.0	67.1	92.5	200.4	35.5	13.6
Ta	49.5	170.0	91.2	59.6	210.5	770.0
Tb	0.03	0.04	0.05	0.04	0.06	0.01
Th	0.13	0.40	0.32	0.21	0.45	0.32
Tl	0.7	2.2	2.5	2.3	*bdl*	8.9
Tm	0.02	0.02	0.02	0.02	0.03	0.01
U	1.59	5.51	5.17	5.14	14.47	14.75
V	*bdl*	5	*bdl*	*bdl*	*bdl*	*bdl*
W	2	2	2	1	2	7
Y	0.9	1.6	1.7	1.7	1.9	0.5
Yb	*bdl*	0.10	0.08	0.07	0.10	*bdl*
Zn	8	14	22	11	5	57
Zr	16	23.8	15	9	60	19
K/Rb	43.9	31.4	36.9	42.4	139.4	21.1
K_2O/Na_2O	0.15	0.24	0.62	0.42	0.05	2.33
Nb/Ta	1.2	0.9	1.5	1.3	1.0	2.0

Wall = wall zone. IZ 1 = intermediate zone 1. IZ 2 = intermediate zone 2. IZ 3 = intermediate zone 3. Ab = saccharoidal albite zone. Phy = phyllic alteration

7. Niobium–tantalum oxide composition

Microprobe analyses of the Nb–Ta oxides (averages for zone and style in Tabs 3–4; see the electronic supplement, Tab. S1, for full dataset) indicate they are Fe-rich columbite–tantalite group minerals, although none conform to pure end-members. The total cation content is less than 3.03, which precludes the accommodation of Fe^{3+} in the columbite–tantalite structure. The major-element composition varies widely: 15.0 to 56.8 wt. % Ta_2O_5, 23.4 to 64.0 wt. % Nb_2O_5, and 12.2 to 16.2 wt. % FeO. The Mn content is low, between 2.7 and 5.7 wt. % MnO. In places, there are significant quantities of trace elements present; up to 2.1 wt. % TiO_2, 1.8 wt. % WO_3, 1.2 wt. % SnO, 0.9 wt. % PbO, 0.6 wt. % UO_2, and 0.5 wt. % ZrO_2. Several analyses contained up to 3.7 wt. % of these trace elements combined.

Crystals that display normal zoning are generally ferrocolumbite in composition, whereas oscillatory-zoned crystals are Ti-rich ferrotantalite. The average chemical composition of crystals that display reverse crystal zoning is similar to that of crystals with normal zoning, with a slight difference in Ta from the inner core to the outer core. Finally, complex crystals are composed of heterogeneous ferrotantalite, with variable Ta and Ti concentrations resulting from secondary processes. The complex internal zonation patterns do not display a wide range in compositions unlike the complex multi-phase oxides found in other large pegmatite deposits, including Tanco (Van Lichtervelde et al. 2007).

This study did not examine the structural state of Nb–Ta oxides; however, Nb–Ta species throughout the Yellowknife pegmatite field were analyzed by Wise (1987). This author described little variation in the structural state of the Nb–Ta oxides, with the degree of order ranging between 37 % and 62 %, which is consistent with an intermediate structural state.

8. Muscovite associated with Nb–Ta oxides

8.1. Petrography

Primary muscovite occurs in the wall and intermediate zones, and is intergrown with albite, K- feldspar, quartz, spodumene, and amblygonite–montebrasite (Fig. 6a–c). The distinguishing feature is its coarse grain size (< 0.5 to 10 cm) which is comparable to associated magmatic minerals. This mica is transparent to pale green and tends to be subhedral to euhedral. In general, muscovite crystals are homogenous, lacking chemical zonation, and inclusion-free. The textural relationships indicate that the muscovite was syn- or post- crystallization relative to the columbite–tantalite (Fig. 6a).

Tab. 3 Average EPMA of columbite–tantalite from each pegmatite zone (primary and secondary features), atoms per formula unit (apfu per 6 O)

	Wall Zone			Intermediate Zone 1			Aplitic Albite Zone			
	Primary	Sec. Early Overgrowths	Sec. Late Overgrowths	Primary	Sec. Early Overgrowths	Sec. Late Overgrowths	Primary	Sec. Early Overgrowths	Sec. Late Overgrowths	Sec. Late Replacement
	n = 13	n = 4	n = 1	n = 13	n = 4	n = 1	n = 25	n = 8	n = 7	n = 9
CaO – wt. %	0.02	0.02	0.02	0.0	0.04	0.04	0.03	0.00	0.00	0.03
FeO	15.49	15.29	15.98	15.10	14.16	12.79	14.07	13.20	14.00	14.18
MnO	3.6	3.6	2.8	4.0	4.1	5.7	3.6	3.4	4.0	3.3
MgO	0.06	0.05	0.14	0.00	0.03	0.02	0.05	0.10	0.00	0.04
TiO_2	0.59	0.50	0.61	0.50	0.48	0.69	0.92	0.90	0.90	0.86
Nb_2O_5	60.7	57.3	56.6	61.6	51.5	52.3	44.9	31.7	46.0	43.3
Ta_2O_5	17.4	19.2	18.5	17.8	28.6	26.6	35.2	50.4	34.0	37.1
SnO_2	0.07	0.10	0.02	0.10	0.13	0.11	0.34	0.40	0.30	0.18
WO_3	0.0	0.1	1.8	0.0	0.0	0.1	0.0	0.0	0.3	0.0
PbO	0.77	0.75	0.70	0.80	0.64	0.66	0.57	0.40	0.60	0.55
ThO_2	0.0	0.0	0.0	0.0	0.0	0.0	0.0	0.0	0.0	0.0
UO_2	0.0	0.0	0.0	0.0	0.0	0.0	0.0	0.1	0.0	0.0
Sb_2O_3	0.0	0.0	0.0	0.0	0.0	0.0	0.0	0.0	0.0	0.0
Y_2O_3	0.1	0.0	0.0	0.0	0.0	0.0	0.0	0.0	0.0	0.0
ZrO_2	0.23	0.15	0.00	0.20	0.03	0.00	0.11	0.00	0.00	0.11
Total	98.97	97.11	97.22	100.10	99.71	99.03	99.80	100.50	100.10	99.61
Ca – apfu	0.0	0.0	0.0	0.0	0.0	0.0	0.0	0.0	0.0	0.0
A site	0.00	0.00	0.00	0.00	0.00	0.00	0.00	0.00	0.00	0.00
Fe	0.79	0.81	0.84	0.80	0.76	0.68	0.77	0.80	0.80	0.79
Mn	0.2	0.2	0.1	0.2	0.2	0.3	0.2	0.2	0.2	0.2
Mg	0.01	0.00	0.01	0.00	0.00	0.00	0.00	0.00	0.00	0.00
B site	0.99	1.00	1.01	1.00	0.98	0.99	0.98	1.00	1.00	0.97
Ti	0.03	0.02	0.03	0.00	0.02	0.03	0.05	0.00	0.00	0.04
Nb	1.7	1.6	1.6	1.7	1.5	1.5	1.3	1.0	1.4	1.3
Ta	0.3	0.3	0.3	0.3	0.5	0.5	0.6	1.0	0.6	0.7
Sn	0.00	0.00	0.00	0.00	0.00	0.00	0.01	0.00	0.00	0.00
W	0.0	0.0	0.0	0.0	0.0	0.0	0.0	0.0	0.0	0.0
Pb	0.01	0.01	0.01	0.00	0.01	0.01	0.01	0.00	0.00	0.01
U	0.0	0.0	0.0	0.0	0.0	0.0	0.0	0.0	0.0	0.0
Y	0.0	0.0	0.0	0.0	0.0	0.0	0.0	0.0	0.0	0.0
Zr	0.01	0.00	0.00	0.00	0.00	0.00	0.00	0.00	0.00	0.00
C site	2.02	2.01	2.00	2.00	2.02	2.02	2.03	2.00	2.00	2.03
Total	3.01	3.02	3.01	3.00	3.00	3.01	3.00	3.00	3.00	3.00
Mn/(Mn + Fe)	0.19	0.19	0.15	0.20	0.23	0.31	0.21	0.20	0.20	0.19
Ta/(Ta + Nb)	0.15	0.17	0.16	0.10	0.25	0.23	0.32	0.50	0.30	0.34

apfu = atoms per formula unit

Tab. 4 Average EPMA of columbite–tantalite from each style of internal zonation (primary and secondary features) (apfu per 6 O)

	Normal Zoning		Normal Zoning. Multiple Overgrowths			Reverse Zoning			Oscillatory Zoning		Complex Zoning	
	Unzoned core. Medium-grey	Overgrowths. Light	Unzoned Core. Veiny	Overgrowths. Light	Overgrowths. Medium-Grey	Inner Core. Light	Outer Core. Medium	Replacement. Light	Zoned Core. Light	Replacement. Dark	Core. Light to Medium	Replacement. Dark
wt. %	n = 15	n = 3	n = 13	n = 9	n = 9	n = 2	n = 2	n = 1	n = 14	n = 10	n = 2	n = 1
CaO	0.01	0.01	0.02	0.05	0.03	0.02	0.02	0.02	0.05	0.03	0.05	0.04
FeO	15.26	14.34	15.11	13.53	14.10	15.07	15.17	15.16	12.94	14.04	13.33	12.78
MnO	3.87	4.22	3.90	3.31	4.03	3.78	3.86	3.84	3.05	3.28	3.04	3.40
MgO	0.05	0.03	0.04	0.07	0.04	0.03	0.01	0.02	0.07	0.04	0.09	0.04
TiO_2	0.52	0.48	0.63	0.72	0.87	0.79	0.51	0.50	1.51	0.91	1.09	1.37
Nb_2O_5	61.36	55.19	58.46	35.24	47.84	58.52	58.87	58.46	28.65	41.99	31.30	29.93
Ta_2O_5	17.68	24.56	20.40	46.28	31.45	18.81	17.82	18.51	51.96	38.43	49.59	50.72
SnO_2	0.07	0.13	0.10	0.30	0.21	0.10	0.07	0.09	0.79	0.23	0.53	0.77
WO_3	0.00	0.00	0.00	0.00	0.48	0.00	0.10	0.09	0.00	0.00	0.00	0.00
PbO	0.79	0.69	0.74	0.42	0.60	0.75	0.77	0.79	0.35	0.53	0.36	0.35
ThO_2	0.00	0.00	0.00	0.00	0.00	0.00	0.00	0.00	0.00	0.00	0.00	0.01
UO_2	0.01	0.00	0.02	0.06	0.00	0.00	0.02	0.06	0.00	0.00	0.00	0.00
Sb_2O_3	0.00	0.00	0.00	0.00	0.00	0.00	0.00	0.00	0.00	0.00	0.00	0.00
Y_2O_3	0.05	0.01	0.05	0.00	0.01	0.02	0.04	0.03	0.00	0.00	0.00	0.00
ZrO_2	0.15	0.04	0.15	0.01	0.03	0.48	0.19	0.19	0.10	0.11	0.04	0.07
Total	99.82	99.69	99.63	99.99	99.69	98.37	97.44	97.75	99.47	99.60	99.40	99.48
Ca – apfu	0.00	0.00	0.00	0.00	0.00	0.00	0.00	0.00	0.00	0.00	0.00	0.00
A site	0.00	0.00	0.00	0.00	0.00	0.00	0.00	0.00	0.00	0.00	0.00	0.00
Fe	0.78	0.75	0.78	0.78	0.76	0.78	0.79	0.79	0.77	0.78	0.78	0.76
Mn	0.20	0.22	0.20	0.19	0.22	0.20	0.20	0.20	0.18	0.19	0.18	0.20
Mg	0.00	0.00	0.00	0.01	0.00	0.00	0.00	0.00	0.01	0.00	0.01	0.00
B site	0.98	0.98	0.99	0.98	0.99	0.98	1.00	1.00	0.96	0.97	0.98	0.96
Ti	0.02	0.02	0.03	0.04	0.04	0.04	0.02	0.02	0.08	0.05	0.06	0.07
Nb	1.69	1.56	1.63	1.10	1.40	1.64	1.66	1.65	0.92	1.27	1.00	0.96
Ta	0.29	0.42	0.34	0.87	0.55	0.32	0.30	0.31	1.01	0.70	0.95	0.98
Sn	0.00	0.00	0.00	0.01	0.01	0.00	0.00	0.00	0.02	0.01	0.01	0.02
W	0.00	0.00	0.00	0.00	0.01	0.00	0.00	0.00	0.00	0.00	0.00	0.00
Pb	0.01	0.01	0.01	0.01	0.01	0.01	0.01	0.01	0.01	0.01	0.01	0.01
U	0.00	0.00	0.00	0.00	0.00	0.00	0.00	0.00	0.00	0.00	0.00	0.00
Y	0.00	0.00	0.00	0.00	0.00	0.00	0.00	0.00	0.00	0.00	0.00	0.00
Zr	0.00	0.00	0.00	0.00	0.00	0.01	0.01	0.01	0.00	0.00	0.00	0.00
C site	2.02	2.02	2.02	2.02	2.02	2.03	2.01	2.01	2.04	2.03	2.03	2.04
Total	3.00	3.00	3.01	3.00	3.01	3.01	3.01	3.01	3.00	3.00	3.01	3.00
Mn/(Mn + Fe)	0.20	0.23	0.21	0.20	0.22	0.20	0.20	0.20	0.19	0.19	0.19	0.21
Ta/(Ta + Nb)	0.15	0.21	0.17	0.44	0.28	0.16	0.15	0.16	0.52	0.36	0.49	0.50

apfu = atoms per formula unit

In general, secondary muscovite is much finer grained than primary one, although several coarser crystals were observed, and in many of the zones it replaces previous minerals (usually feldspars), and occurs as veins or fracture fillings (Fig. 6d–f). It is abundant in the border zone, aplitic albite zone, and phyllic alteration after intermediate zones. It is less common in the wall and intermediate zones. Crystal sizes range from < 0.05 to 0.5 cm and they are transparent, brown, or green, anhedral, and commonly contain mineral inclusions of feldspar and columbite–tantalite.

8.2. Major- and trace-element composition

The average chemical composition of muscovite from each of the zones is given in Tab. 5; the supplementary full dataset (Tab. S2) and a comparison of trace-element contents in muscovite throughout the pegmatite field (Tab. S3) are available online. The compositions are close to end-member dioctahedral muscovite, ideally $KAl_2(AlSi_3)O_{10}(OH,F)_2$, as the lithium content in the mica is too low to be classified as lithian muscovite. On average, there is minor Fe (avg. 0.55 wt. % FeO), Na (avg. 0.52 wt. % Na_2O), and Mg (avg. 0.25 wt. % MgO), with uniform silica (44.83–46.42 wt. % SiO_2) and Al (34.70–38.84 wt. % Al_2O_3).

Within all muscovites, the minor-element content is low (Ti up to 0.50 wt. % TiO_2). The relative concentrations of trace-elements in primary and secondary muscovite, along with values from whole-rock geochemistry, are represented as box-and-whisker plots in Fig. 7. The primary muscovite contains elevated concentrations of Li (avg. 247.4 ppm), Cs (avg. 134.8 ppm), Ta (avg. 88.5 ppm), Be (avg. 17.6 ppm), Nb (avg. 76.4 ppm), Sn (avg. 398.7 ppm), Rb (avg. 4824.9 ppm), Sr (avg. 5.5 ppm), and Ba (avg. 150.0 ppm). Compared to the primary generation, the secondary muscovite has higher average concentrations of Nb (avg. 194.6 ppm), B (avg. 83.3 ppm), and Zn (avg. 113.6 ppm), and relatively lower Ta (avg. 38.8 ppm), Cs (avg. 88.5 ppm), Li (avg. 151.7 ppm), Sr (avg. 1.6 ppm), and Ba (avg. 10.2 ppm).

At the scale of an individual muscovite grain, the major-element composition is relatively homogenous; however, strong enrichment of Al, Rb, K, and Cs near grain margins is common, which is accompanied by a sharp increase in the K/Rb ratio. This increase (3–5× compared to the inner parts of the crystal) is too large to be attributed to normal fractionation and, instead, may be due to late-stage reaction processes. These rims were not evident either under optical microscope or in the BSE imagery. In general, such a rimward K/Rb decrease is similar to that documented

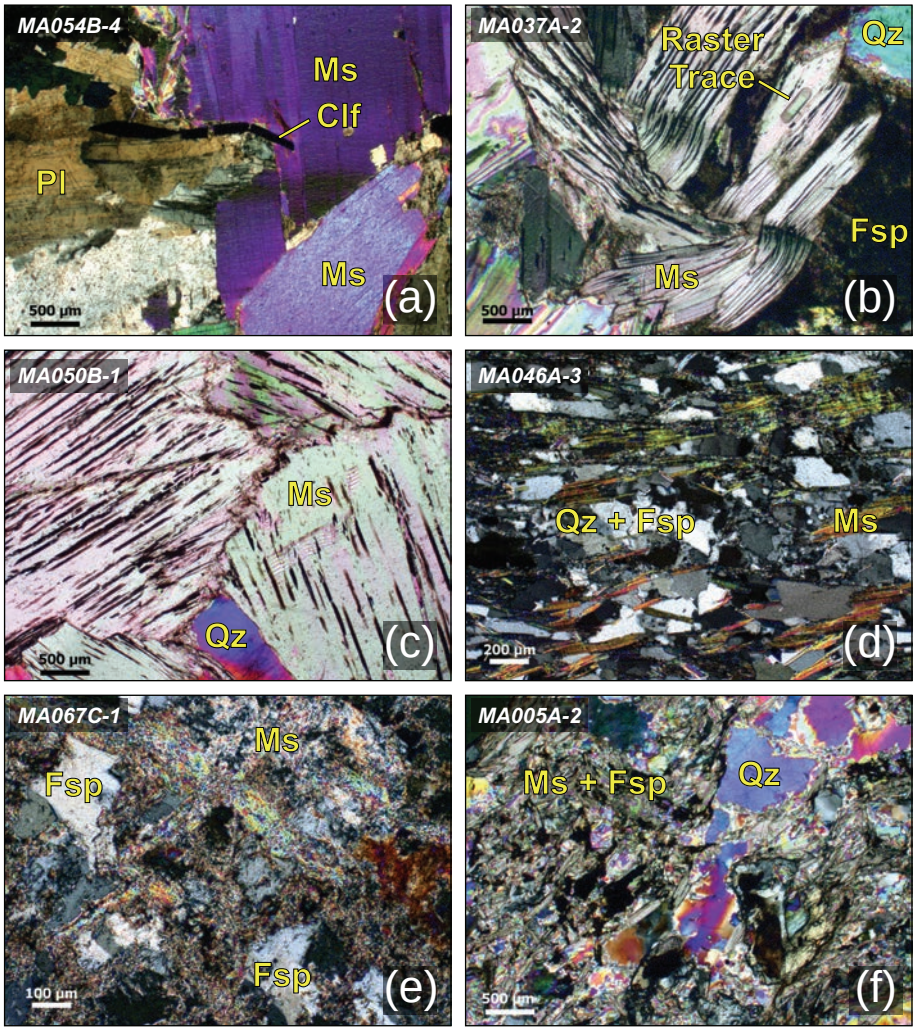

Fig. 6 Photomicrographs of muscovite, cross-polarized transmitted light. Primary muscovite (a–c) is characterized by large crystal sizes (< 7 cm), subhedral shape, equigranular texture, and lack of inclusions. Secondary muscovite (d–f) shows a finer crystal size, anhedral shape, abundant inclusions, and may have a linear fabric. **a –** Primary muscovite; the muscovite post-dates the columbite–tantalite (opaque mineral, centre). **b –** Primary muscovite; effects of crystal deformation and raster traces of LA ICP-MS analyses are both visible. **c –** Very coarse-grained primary muscovite. **d –** Fine-grained secondary muscovite with linear alignment. **e –** Very fine-grained secondary muscovite replacing earlier feldspars. **f –** Very fine-grained secondary muscovite.

Tab. 5 Average LA ICP-MS analyses and their corresponding electron-microprobe analyses of muscovite for each mineralogical zone (ppm)

	Phyllic Alteration		Wall Zone		Inter. Zone 1		Inter. Zone 2		Inter. Zone 3
	Pr	Sec	Pr	Sec	Pr	Sec	Pr	Sec	Pr
	n = 13	n = 6	n = 3	n = 1	n = 16	n = 18	n = 3	n = 18	n = 10
EPMA									
SiO_2 – wt.%	45.74	45.57	45.44	45.45	45.57	45.84	45.64	45.77	45.53
TiO_2	0.19	0.01	0.03	0	0.02	0.09	0.22	0.03	0.04
Al_2O_3	36.83	38.22	38.17	37.63	38.37	38.36	35.59	38.21	38.30
FeO	0.78	0.44	0.40	0.59	0.35	0.39	1.39	0.44	0.37
MnO	0.00	0.00	0.00	0	0.00	0.00	0.00	0.00	0.00
MgO	0.58	0.04	0.02	0.03	0.03	0.06	0.92	0.05	0.05
CaO	0.03	0.01	0.02	0	0.02	0.04	0.02	0.04	0.02
Na_2O	0.58	0.66	0.49	0.63	0.51	0.72	0.46	0.62	0.48
K_2O	9.23	9.21	9.52	9.28	9.37	9.13	9.48	9.12	9.47
BaO	0.09	0.02	0.03	0.00	0.01	0.01	0.15	0.03	0.01
Cs_2O	0.01	0.01	0.00	0.03	0.01	0.01	0.03	0.01	0.02
F	0.06	0.06	0.03	0.01	0.03	0.03	0.15	0.07	0.07
Cl	0.01	0.01	0.00	0.01	0.01	0.01	0.00	0.01	0.00
Li_2O calc	0.06	0.06	0.04	0.02	0.04	0.03	0.13	0.06	0.07
H_2O calc	4.47	4.49	4.49	4.48	4.51	4.53	4.40	4.50	4.49
O=F, Cl	0.03	0.03	0.01	0.01	0.02	0.01	0.06	0.03	0.03
LA–ICP–MS									
std Al_2O_3	37.34	38.69	38.68	38.34	38.82	38.66	36.13	38.62	38.73
SiO_2 – wt.%	37.14	38.70	36.27	35.60	38.78	40.05	36.60	38.98	37.67
FeO	0.28	0.22	0.22	0.37	0.24	0.20	0.71	0.25	0.15
MgO	0.65	0.03	0.02	0.03	0.03	0.06	1.11	0.06	0.05
Na_2O	0.48	0.54	0.37	0.42	0.48	0.75	0.42	0.61	0.40
K_2O	10.83	11.00	10.32	9.86	11.34	11.06	12.17	11.17	11.03
Rb_2O	0.37	0.54	0.40	0.990	0.52	0.39	0.86	0.58	0.48
Li – ppm	425.53	127.78	68.90	101.00	164.34	147.54	898.00	163.81	238.53
Be	15.94	21.02	12.00	28.70	18.08	21.24	21.93	19.88	17.17
B	34.02	79.07	34.00	118.00	49.24	79.71	53.70	88.32	57.55
Ti	1174.61	115.05	161.13	49.20	156.91	449.01	2404.33	160.65	227.89
Mn	32.13	42.97	42.81	153.00	39.92	30.36	42.33	49.56	33.77
Zn	42.33	103.33	48.03	346	71.85	99.80	36.93	130.86	61.16
Sr	43.35	0.33	0.50	0.1	1.10	1.70	48.07	1.90	1.26
Zr	0.72	0.47	0.10	0.79	0.24	0.77	0.58	0.54	0.24
Nb	118.44	181.13	56.22	159.2	76.99	208.20	106.53	185.44	72.56
Sn	373.31	286.43	369.87	890.00	331.54	194.70	728.37	358.63	416.01
Sb	0.08	0.07	0.06	0.04	0.08	0.07	0.05	0.06	0.05
Cs	133.67	83.75	59.26	258.50	91.82	51.60	342.67	120.05	163.70
Ba	524.31	0.90	13.17	0.40	7.32	8.51	1513.67	15.07	10.24
Ta	131.78	36.95	54.54	65.30	87.39	32.69	146.87	45.49	82.90
K/Rb	27.81	18.55	23.44	9.05	22.58	25.66	12.92	19.17	21.23
K/Cs	1064.13	1099.77	1451.22	316.67	1291.47	1819.58	296.50	1092.13	732.30
Nb/Ta	0.91	4.93	1.04	2.4	1.18	7.30	0.73	4.65	0.95
Li/Cs	3.22	1.56	1.20	0.39	2.39	2.97	2.62	1.94	1.96
Rb/Cs	39.63	59.23	62.26	35.0	56.14	70.74	23.00	52.73	34.90

Pr = Primary, *Sec* = Secondary
Li_2O calculation after Monier and Robert (1986)
H_2O calculation after Tindle and Webb (1990)
Calculation: (0.31134×F)–0.075895 (Monier and Robert 1996)

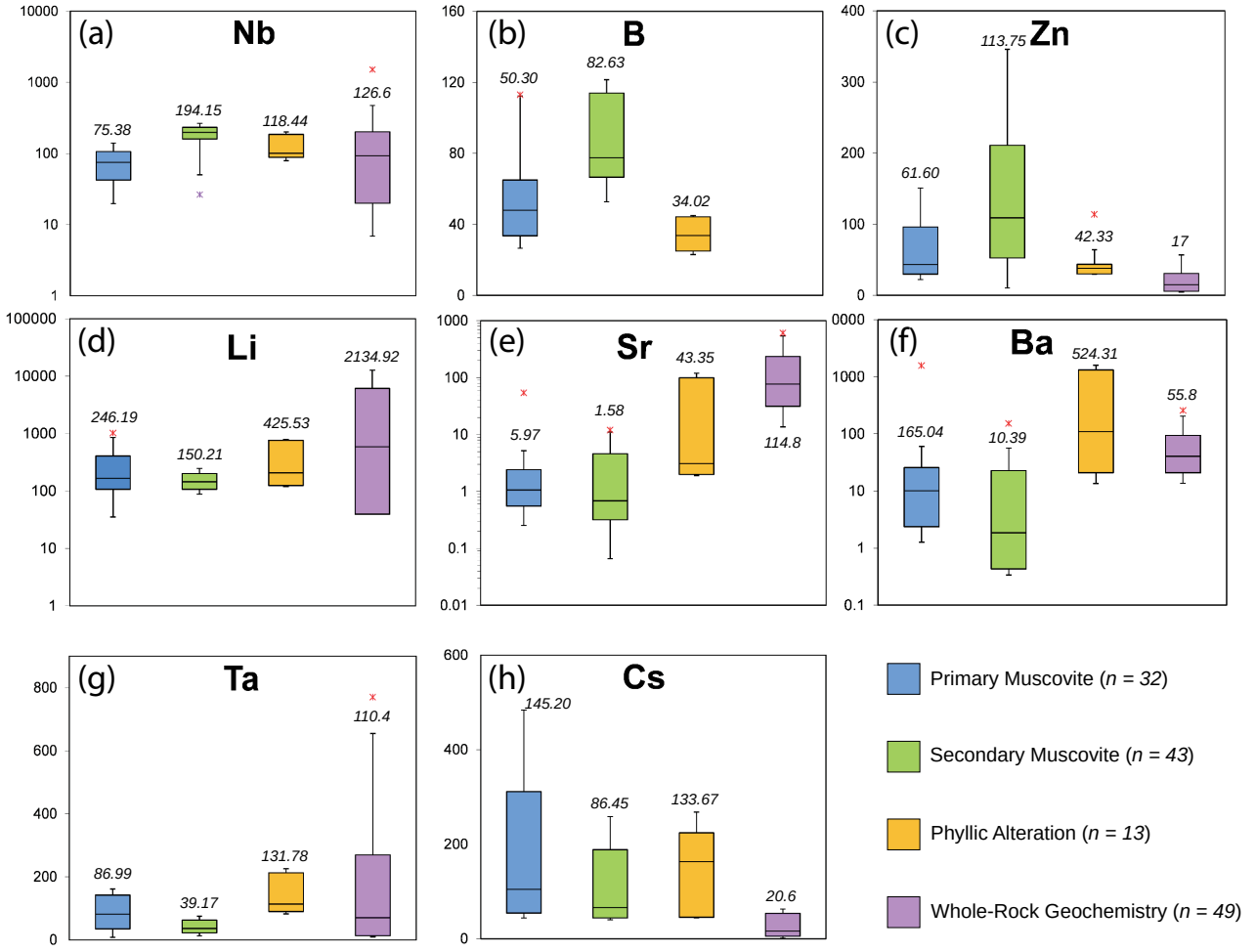

Fig. 7 Box and whiskers plots for chemistry of primary muscovite (blue), secondary muscovite (green), and phyllic alteration muscovite (yellow) analyzed *in situ* by EPMA and LA ICP-MS, along with whole-rock geochemistry data (pink) obtained by ICP-MS. 'Whiskers' represent the range of data, without outliers indicated by *. The top of the 'box' represents the 90th percentile, its bottom the 10th percentile and the middle line is the median value. Relative to the primary generation, the secondary muscovite is enriched in: **a –** Niobium (logarithmic scale), **b –** Boron and **c –** Zinc; and is relatively depleted in: **d –** Lithium (logarithmic scale), **e –** Strontium (logarithmic scale), **f –** Barium (logarithmic scale), **g –** Tantalum, and **h –** Cesium.

in muscovites from other pegmatites, including Tanco (e.g., Van Lichtervelde et al. 2008).

9. Discussion

9.1. Chemical evolution of muscovite

The K/Rb ratio in muscovite is a useful indicator of pegmatite evolution and is expected to decrease with progressive fractionation (London 2008). As shown in Tab. 5, this ratio decreases from the wall zone, to intermediate zones 1, 3, and then 2. This is consistent with crystallization of the pegmatite from the margins inwards. Similarly, pegmatite fractionation is also demonstrated by the Nb/Ta ratio, as shown in Fig. 8a–c, which reveals the same sequence of fractionation between pegmatite zones. Secondary muscovites (all zones; circled by a thick dashed line) are distinct from the primary generation by containing low Ta, and high Nb (Fig. 8a), as well as low Li contents and a broad range of Nb/Ta values, much greater than those encountered in the primary micas (Fig. 8b).

9.2. Nb–Ta oxide origins: magmatic vs. metasomatic crystallization

9.2.1. Nb–Ta mineral evolution and paragenesis

The assemblage of Nb–Ta minerals in the Moose II pegmatite is relatively simple, consisting exclusively of ferrocolumbite and ferrotantalite. Linnen and Cuney

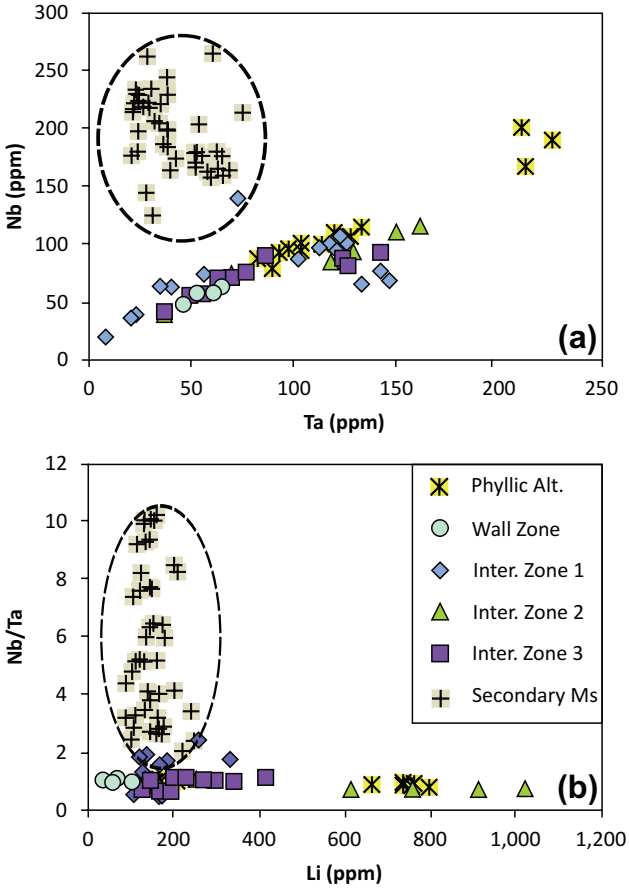

Fig. 8 Correlation diagrams between selected trace-elements (n = 98): **a –** Fractionation between Nb and Ta, **b –** Nb/Ta fractionation with increasing Li. Analyses of secondary muscovite (all zones) are outlined by a thick dashed line.

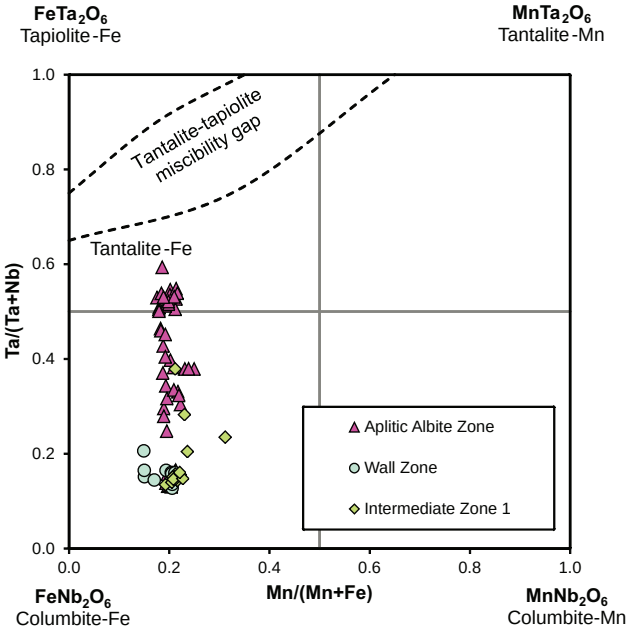

Fig. 9 Electron-microprobe data (apfu) plotted in the columbite–tantalite quadrilateral (after Černý et al. 1986) showing the evolution of the Nb–Ta oxides between different pegmatite zones (n = 78).

(2005) reviewed the solubility of Nb and Ta in granitic melts, even at subsolidus temperatures, and noted that it increases with temperature, alkalinity, and the abundance of fluxing elements in the melt. Furthermore, they also noted that the increase in Ta relative to Nb can be explained by the higher tantalite solubility relative to columbite at higher temperatures. Bartels et al. (2010) demonstrated that the solubility of columbite–tantalite is enhanced by the presence of Li, F, B, and P in the melt; therefore, columbite should precipitate earlier than tantalite. As a result of this fractional crystallization, the ratio of Ta/(Ta + Nb) will increase in the melt and this can be observed at scales ranging from individual pegmatite zones to individual columbite–tantalite crystals. Application of whole-rock data to assess the relative fractionation of pegmatite zones is limited by the size of bulk samples collected relative to the crystal size, and thus may not be representative of the melt composition. For this reason columbite–tantalite crystal chemistry is the preferred method of analysis. Concurrent with the adjustments in the Ta–Nb concentrations, Mn is generally enriched relative to Fe during the fractionation of a pegmatite melt (Černý and Ercit 1985). The enrichment of Mn in the melt is enhanced by the high activity of fluorine (Černý et al. 1986). Thus, fractional crystallization causes the evolution of columbite–tantalite from ferrocolumbite [$FeNb_2O_6$] to manganotantalite [$MnTa_2O_6$] (e.g., Novák et al. 2003; London 2008; Chudík et al. 2011), as shown in plots of Ta* [Ta* = Ta/(Ta + Nb)] *versus* Mn* [Mn* = Mn/(Mn + Fe)], after Černý et al. (1986).

At the pegmatite-scale, the EPMA analyses of columbite–tantalite show an evolution from Nb- to Ta-rich, progressing from the wall to the intermediate and aplitic albite zones (Tab. 3; Fig. 9). The Ta* contents in the Moose II pegmatite range from 0.13 to 0.59, occupying a wider range than has been documented by previous work on Nb–Ta oxides in the Yellowknife Pegmatite Field (Ta* = 0.14 to 0.32; Wise 1987). Similarly, the results show a slight increase in the Mn* values from the wall zone to the intermediate zones (0.15–0.31). In granitic pegmatites, the Mn* ratio is controlled in large part by the crystallization of tourmaline (London 2008). However, in the Moose II pegmatite, tourmaline mineralization is rare and occurs only where metasomatic reactions involving the host metasediments took place. Consequently, the evolution of Mn–Fe in the Moose II melt can be attributed to the crystallization of muscovite and columbite–tantalite, resulting in a narrow range of compositions. This is consistent with Mn* values obtained for Nb–Ta oxides throughout Yellowknife pegmatite field (Mn* = 0.18–0.27; Wise 1987).

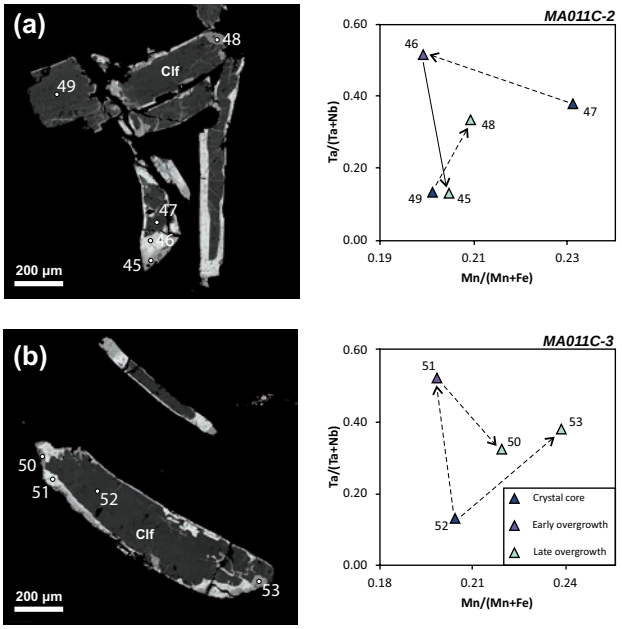

Fig. 10 Back-scattered electron images of normal crystal zoning and overgrowths in ferrocolumbite, with EPMA compositions (apfu) plotted in the columbite–tantalite quadrilateral (Černý et al. 1986), and the location of the probe points indicated. Dashed arrows connect phases that are spatially associated, solid ones indicate continuous evolution between phases. **a –** Ferrocolumbite with early Ta-rich (point 47) and late Nb-rich (points 45 and 48) overgrowths and veinlets. **b –** Ferrocolumbite with early Ta-rich (point 51) and late Nb-rich (points 50 and 53) overgrowths. The Nb-rich phases have higher Ta* values compared to the primary crystals.

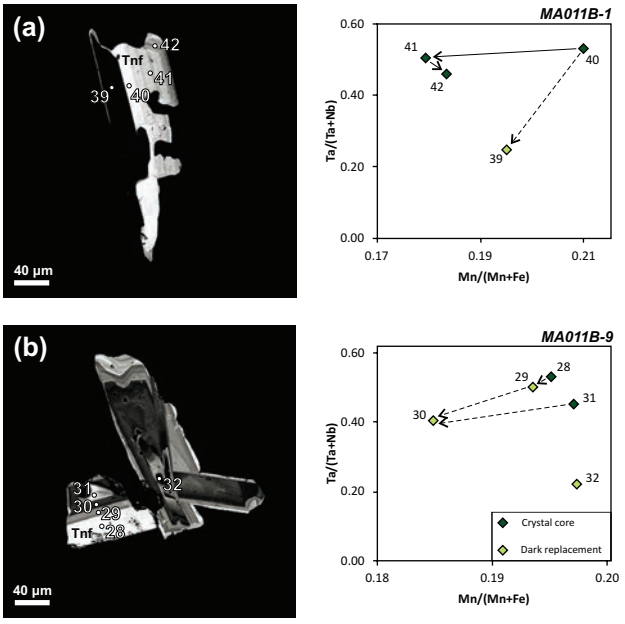

Fig. 11 Back-scattered electron images of oscillatory zoned crystals and irregularly zoned patchy replacement in ferrotantalite, with electron microprobe compositions (apfu) plotted in the columbite–tantalite quadrilateral and the location of the probe points indicated. Dashed arrows connect phases that are spatially associated, solid ones indicate continuous evolution between phases. **a –** Ferrotantalite with early oscillations (points 41 and 42) truncated by later oscillations (point 42), becoming slightly enriched in Nb relative to Ta from the core to the rim of the crystals. Nb-rich patchy replacement displays very weak zonation (point 39). **b –** Ferrotantalite with complex oscillations and replacement. It is difficult to distinguish primary phases from replacement ones; the Ta-rich rim (point 28) appears to be overgrown by Nb- rich phases (points 29 and 30), based on the planar contact.

The chemical trends for normally-zoned crystals are shown in Fig. 10a–b. Textural evidence supports a clear association of a Ta-rich phase overgrowing euhedral ferrocolumbite (points 46 and 51). In some instances, a second generation of overgrowths is seen, enriched in Nb relative to Ta (points 45, 48, 50 and 53). These Nb–W-rich overgrowths replace the primary crystals, as well as the earlier Ta-rich overgrowths. Late veins or fracture fillings (either Ta- or Nb-rich) occasionally crosscut crystals. The chemical trends for oscillatory-zoned ferrotantalite crystals (Fig. 11a–b) are complicated by truncations of earlier oscillations by later ones (Fig. 11a), with a progressive decrease in Ta* that is contrary to normal fractionation patterns (point 42). Oscillatory zoning may indicate a change in magma composition between successive pulses or changes in intensive parameters in the parental liquid. In some cases, complex zoning patterns make distinguishing primary from replacement phases difficult. Finally, late Nb-rich patchy replacement always overprints the earlier oscillatory zoning, and rarely displays weak zonation (points 39 and 32). The relative timing of crystallization of the Nb–Ta oxides is shown in Fig. 12. The degree of fractionation of the Nb–Ta oxides is below that of the world-class Tanco pegmatite, Manitoba, Canada, which is characterized by the presence of

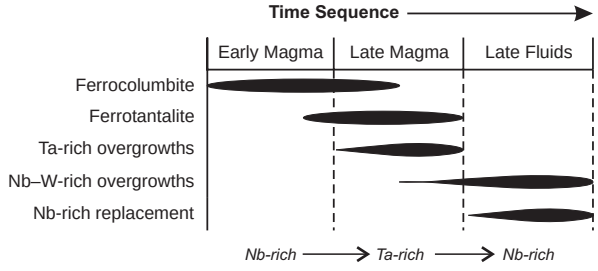

Fig. 12 Sequence of crystallization of Nb–Ta oxide phases interpreted from textural and chemical evidence. Enrichment in Ta or Nb is relative to the earlier phases.

manganotantalite, manganowodginite, and tapiolite (e.g., Van Lichtervelde et al. 2007).

9.2.2. Magmatic origins

The textural features of the Nb–Ta oxides can be used to distinguish primary magmatic from metasomatic features. In magmatic systems, the Nb–Ta oxides tend to be euhedral and have simple crystal zoning patterns. Composi-

tional zoning within individual crystals indicates ongoing chemical communication with an evolving parental melt during the crystallization of the pegmatite. Normal and oscillatory zoning patterns of columbite–tantalite crystals in assemblages of primary magmatic minerals are thought to be due to non-equilibrium or changing equilibrium conditions during fractional crystallization (Lahti 1987; Černý et al. 1992). Oscillatory zoning may be caused by the slow diffusion of Nb and Ta in the melt relative to the rate of crystal growth (Lahti 1987). Alternatively, the difference in solubility between the columbite and tantalite end-members determines the threshold saturation for crystal nucleation under supersaturated conditions, which may facilitate the formation of oscillatory zoning, regardless of changes in melt composition (Putnis et al. 1992). Furthermore, the behaviour of Nb and Ta in the melt may play an important role, as the latter preferentially complexes with F than hydroxyl ions, resulting in differential solubilities as the melt evolves (Černý et al. 1985).

In the Moose II pegmatite, the oscillatory and normally zoned crystals are the most common. Their euhedral shapes in sharp contact with primary minerals, such as quartz and feldspar, suggest that these mineralization styles may be interpreted to result from the primary magmatic crystallization. The truncation of some early-formed by later oscillatory crystal zones (see Fig. 5c–d) may have resulted from successive pulses of magma entering a dilating intrusion channel. Similarly, the reverse crystal zoning may reflect a slight change in magma composition, precipitating Nb-rich columbite over a relatively Ta-rich core.

9.2.3. Magmatic–metasomatic origins

The term "metasomatic" refers to the replacement of primary features, but does not indicate whether the metasomatic fluid was magmatic or hydrothermal (i.e., aqueous). Whole-rock geochemistry reveals an important association of Nb and Ta with muscovite- and albite-rich portions of the pegmatite (Fig. 13; after Kontak 2006). The lack of correlation of rare-elements with primary K-feldspar and spodumene suggests that metasomatism may have been the dominant process of Nb and Ta enrichment. Therefore, distinguishing magmatic *versus* hydrothermal metasomatism is important in understanding the genesis of the Nb–Ta oxides.

The metasomatic replacement and alteration of primary Nb–Ta oxide minerals results in a complex variety of secondary phases, as concentration of elements in late fluids may cause the crystallization of additional minerals. This complex internal zonation patterns generally occur in late muscovite- or albite-rich replacement units (e.g., Černý 2005; Kontak 2006; Van Lichtervelde et al. 2007). Similarly, in the Moose II pegmatite the complex

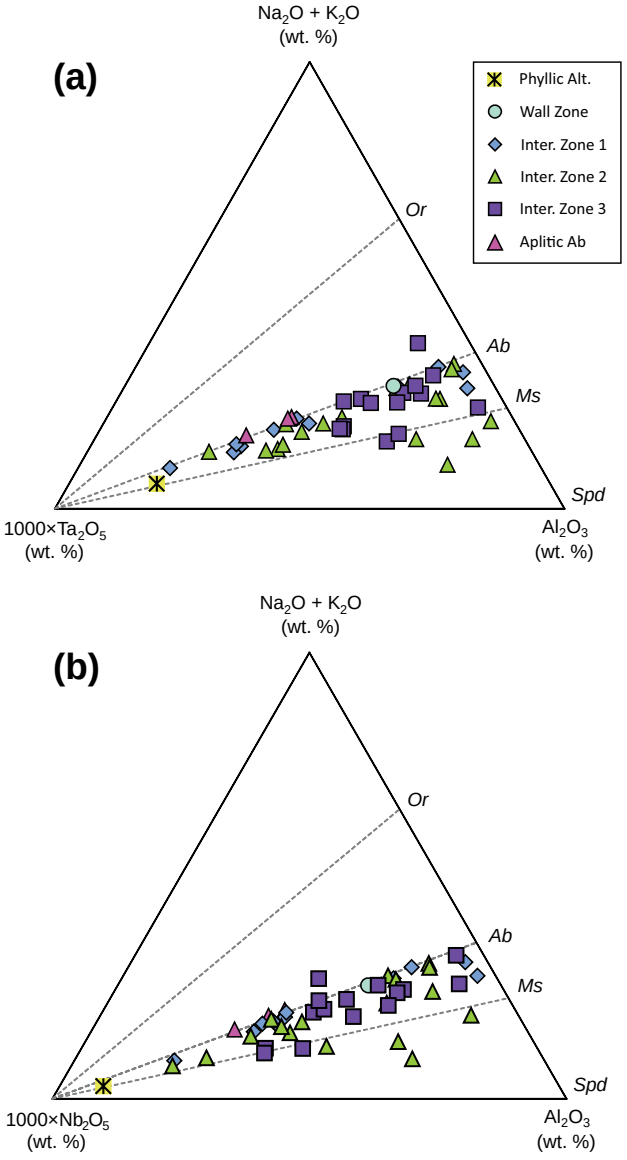

Fig. 13 Ternary plots of the whole-rock geochemical data from the Moose II pegmatite (n = 49). This figure demonstrates the association of Ta (**a**) and Nb (**b**) enrichments with the albite- and muscovite-rich parts of the pegmatite. Tie lines are based on compositions of mineral phases in the pegmatite.

oxides in the phyllic alteration and aplitic albite zones are Ti-rich ferrotantalite surrounded by later, more evolved (Ta- rich) generation of the same mineral. These chemical features, along with the presence of sieve and embayment textures, are interpreted to represent partial dissolution and recrystallization of the early phases. In general, it is accepted that such replacement features result from the interaction and re-equilibration with later metasomatizing fluids, but the origin of these fluids is still under debate.

The origin of the phyllic alteration in the Moose II pegmatite can be explained in part by magmatic metasomatism coeval with the formation of late aplitic albite

zones. In sharp contrast to many pegmatite zones, the late albite units are very fine-grained with a saccharoidal texture. This indicates rapid nucleation of the minerals, which may result from a pressure-quench. During this process, the confining pressure of the volatile-rich albitic melt increases until fractures develop and pressure suddenly drops (Wood and Williams-Jones 1993) and abundant volatiles are suddenly released, reacting with earlier crystallized units (Tindle and Breaks 2000).

An alternative model suggests that the stabilization of B-, P-, Li-rich minerals, such as spodumene and amblygonite–montebrasite, may reduce the solubility of H_2O in the residual melt, therefore raising the solidus and resulting in rapid nucleation of aplitic zones (London 1987, 1990). This 'chemical quenching' also leads to the exsolution of a hydrous supercritical fluid (London 1990).

By either model, exsolution of volatiles during the formation of the aplitic albite 'pod' in the north section of the Moose II pegmatite was likely responsible for the phyllic alteration adjacent to it (see insert, Fig. 2). In the south section, the phyllic alteration is not associated with aplitic albite zones (see the next insert, Fig. 2). The southern zones are, however, associated with elongated rafts of the host rock, oriented parallel to the pegmatite–wallrock contact, which suggests that successive pulses of magma were injected along a structural feature. As these new melts were injected next to previously crystallized pegmatite, they could have reacted with the K-feldspar of the older pegmatite unit, resulting in muscovite replacement where the bulk composition of the new melt was significantly modified due to the interaction with the rafts of host rock (i.e., magmatic–metasomatism). Increased peraluminosity and high F contents promote the stability of muscovite over orthoclase (Veksler and Thomas 2002). Such a melt could have been extremely enriched in Ta, due to volatile elements that are known to sharply increase Nb–Ta solubilities (Linnen 1998). Indeed, the late phyllic alteration zones contain the highest whole-rock concentrations of Ta and Nb (up to 770 ppm and 1520 ppm, respectively) in the pegmatite. The high K/Rb ratios in the phyllic alteration zones indicate that the composition of the later magma pulses was relatively unevolved, compared to the late-stage fluids responsible for the formation of the aplitic albite zones. The implication is that the metasomatic event that produced the mica alteration also likely enriched tantalum and niobium in the system.

Additional features indicative of metasomatism in the Moose II pegmatite include overgrowths on the Nb–Ta phases, Ta-rich veinlets, and the nature of Nb-rich patchy replacement. Multiple generations of overgrowths on primary ferrocolumbite can be identified, as previously described: (1) The first generation is Ta-rich, and affects most of the ferrocolumbite crystals encountered. These overgrowths locally display oscillatory zoning suggesting that it may have precipitated from an evolved (Ta-rich), late-stage magmatic phase. (2) Later Nb–W-rich overgrowths replace earlier overgrowths and primary phases. (3) Late metasomatic alteration also manifests itself as Nb-rich patchy replacement of ferrotantalite. The patchy replacement overprints earlier crystal zones and is characterized by embayment textures. The patchy replacement features are different in Ta* relative to the primary phases, resulting from distinct fluid–melt partition coefficients of Nb and Ta (Chevychelov et al. 2004). The Nb-rich phases may have originated from a late flux-rich melt (magmatic–metasomatism) or a hydrothermal fluid.

In the aplitic albite zones, reactive fluids may have caused the partial resorption of early columbite and new growth of a late Nb-rich phase (Wood and Williams-Jones 1993; Tindle and Breaks 2000). Thus, a magmatic–metasomatic origin for at least some of the Nb-rich replacement found in the Moose II pegmatite can be considered; however, Nb-rich replacement features are observed in all zones of the pegmatite, apart from the late aplitic albite zones, so this magmatic-metasomatic process cannot account for all of the Nb-rich replacement in columbite–tantalite.

9.2.4. Hydrothermal-metasomatic origins

The origin of the Nb-rich metasomatizing fluid described above is indicated by the trace-element geochemistry of fine-grained secondary muscovite throughout the pegmatite. These secondary micas contain higher concentrations of B, Zn, and Nb, relative to the primary muscovite. The highest Zn concentrations in secondary micas (346 ppm Zn) occur in the wall zone. Small sphalerite crystals were observed, commonly in association with other hydrothermal minerals such as pyrite (Anderson 2013). This may indicate an external source of Zn in the hydrothermal fluids. The high Nb concentrations in the secondary muscovite correlate well with the late Nb-rich replacement features of the columbite–tantalite crystals. As shown in Fig. 10b, the replacement of ferrocolumbite is associated with increasing Ta/(Ta + Nb), suggesting that Nb was released during alteration and subsequently incorporated into the fine-grained secondary muscovite. Hence, this late fluid may not have been inherently Nb-rich.

The low Ta, Cs, Li, Sr, and Ba, along with high B, Zn, and Nb contents, suggest that this fine-grained muscovite crystallized or recrystallized (feldspar hydrolysis reaction product) from an F-rich aqueous (hydrothermal) fluid that may have existed at the same time as the late LCT-rich melt as an immiscible phase. This fluid appears to have remobilized significant quantities of Nb, and little Ta, as is suggested by the Nb-rich nature of the replacement in columbite–tantalite. The remobilization of elements from the primary columbite–tantalite following pegmatite

consolidation are in agreement with work by Van Lichtervelde et al. (2008).

9.3. Experimental constraints

Recent solubility experiments have raised an important issue regarding the crystallization of tantalite in pegmatite-forming melts. Based on the high solubility of Ta, saturation of tantalite in a melt is not achieved until ~2,000 ppm Ta is reached (Linnen and Cuney 2005). This value is much higher than the bulk composition of most tantalite-bearing pegmatites. Experimental work by Linnen and Cuney (2005) demonstrated that in hydrous metaluminous granitic melts a significant undercooling ($T < \sim 530\,°C$) promotes a decrease in the solubility of Nb, resulting in the precipitation of columbite. However, London (2008) proposed constitutional zone refining (CZR) as an alternative explanation for the crystallization of Nb–Ta oxides. As a crystal is growing, the differential rates of element diffusion cause a boundary layer melt to form at the crystal/melt interface. It is characterized by an increase in the concentrations of fluxing and incompatible elements, including Ta (London 2008). In this manner, tantalite saturation is achieved in the boundary layer if the fluxing elements diffuse away faster than Ta. The diffusion rates of Ta have not been examined experimentally, but other HFSE diffusion rates are *c.* 5 orders of magnitude slower than that of F at 450–500 °C (London 2008). Thus, the tantalite enrichment can be driven by fast rates of crystallization in highly undercooled melts. Evidence for boundary-layer saturation is provided by the preferential crystallization of columbite–tantalite along grain boundaries of primary quartz and feldspars.

Finally, tantalite crystallization can be prompted by chemical quenching, i.e. a sudden loss of fluxing elements due to crystallization, diffusion, or removal into a vapour phase (Van Lichtervelde et al. 2007). The crystallization of Li- and F-bearing minerals, particularly spodumene and amblygonite–montebrasite, is likely a significant factor in the precipitation of tantalum minerals at lower temperatures. Van Lichtervelde et al. (2007) suggested that the intergrowth of HFSE-bearing minerals (tantalite, zircon) provides textural evidence for this process.

Experimental studies have suggested that hydrothermal fluids are not able to transport significant quantities of Ta, as reflected by the very low partitioning of Ta (and Nb) between an aqueous fluid and granite melt (Chevychelov et al. 2004, 2005, 2010). Transport of large quantities of Nb (and Ta) can only occur in concentrated F-rich solutions (Keppler 1993; Linnen and Keppler 1997; Linnen 1998; Zaraisky et al. 2010). Aqueous fluoride-rich fluids are, therefore, unable to remove Nb and Ta from the melt, but they may dissolve previously crystallized columbite–tantalite and thereby allow for mobilization and redeposition of these elements (Zaraisky et al. 2010). This latter experimental work also demonstrated that the solubility of Ta is not sensitive to the changes in P–T conditions typical of pegmatite crystallization (300–550 °C and 50–100 MPa). Further experimental studies have demonstrated that melt phases and a hydrous fluid may co-exist, with high F-contents in the late melt resulting in the alteration of K-feldspar to muscovite (Veksler and Thomas 2002). This suggests that hydrothermal fluids could have led to the preferential remobilization of Nb over Ta in the Moose II pegmatite, but it seems unlikely that these fluids enriched the overall contents of the pegmatite over the initial melt composition.

9.4. The role of albitization

The late-stage aplitic albite zones play a minor role in Nb–Ta enrichment due to their limited extent; however, albite metasomatism is pervasive in the intermediate zones. These metasomatic reactions involve alkali exchange between a Na-rich medium and K-feldspars due to gradients in chemical potentials and temperature (London and Morgan 2004; London 2005), which results in replacement of early K-feldspar with late-stage, pink cleavelandite (platey variety of albite). The K released in these reactions could contribute to the formation of secondary muscovite (increase in aK/aNa) via hydrolysis reactions due to the low pH of the fluid (London and Morgan 2004).

London and Morgan (2004) suggested that the Na-rich metasomatic fluids originate from a late volatile- and Na-rich melt. This model was also invoked to explain the aplitic albite zones in the Brazil Lake pegmatite (BLP), Nova Scotia (Kontak 2006). Similar to the Moose II pegmatite, the BLP shows rare-element enrichment in the albite zones (both saccharoidal and bladed) which prompted Kontak (2006) to conclude that the Nb–Ta oxide mineralization resulted from a magmatic–metasomatic, rather than a hydrothermal, process. In contrast to the Moose II pegmatite, Nb–Ta mineralization in the BLP is restricted to albite–quartz units, which are of limited extent. A similar interpretation for the Moose II pegmatite appears to be less plausible due to the fact that the albitization was pervasive. Thus, it is difficult to establish a simple causal relationship between the albite-forming metasomatic processes and the columbite–tantalite mineralization.

10. Conclusions

The Moose II pegmatite is an important host for Nb–Ta mineralization in the form of iron-rich columbite–tantalite:

(i) Niobium and tantalum were initially concentrated by protracted (extreme) fractional crystallization in a flux-rich melt. The primary crystallization of the Nb–Ta oxides may have resulted from a decrease in temperature, loss of fluxing components, or saturation in the boundary layers of growing crystals as a consequence of diffusion-driven processes.

(ii) Alternatively, the association of columbite–tantalite with cleavelandite suggests that magmatic–metasomatism from a low-density Na-rich melt may also have been the primary cause of Nb–Ta enrichment in the pegmatite.

(iii) Primary Nb–Ta oxide mineralization is characterized by normal, reverse, and oscillatory zoning of columbite–tantalite, as revealed by backscattered electron (BSE) imagery.

(iv) Modification of columbite–tantalite by secondary processes is evident with successive generations of overgrowths (Ta-rich followed by Nb–W-rich) and patchy Nb-rich replacement.

(v) Extreme alteration led to complex patterns of internal zonation, typical of the aplitic albite and phyllic alteration (muscovite-rich replacement) zones in the Moose II pegmatite. These late zones are further enriched in Nb and Ta, indicating that magmatic–metasomatic processes played a role in metal enrichment.

(vi) The latest textural feature which replaced earlier primary columbite–tantalite crystals is Nb-rich. Fine-grained secondary muscovite found throughout the pegmatite is also enriched in Nb, as well as B and Zn, relative to the primary muscovite crystals. This is consistent with mobilization of Nb and it re-precipitation in muscovite from an aqueous (hydrothermal) fluid.

(vii) Fractionation trends of Nb–Ta oxides and muscovite indicate that the pegmatite crystallized from the margins inward, beginning at the wall zone, and progressing from intermediate zone 1, 3, and 2, and followed by the late aplitic albite zones.

Acknowledgements. The authors would like to thank Drs. D. Kontak, M. van Lichtervelde, and P. Uher for their thorough reviews of this manuscript. We are indebted to Drs. D.C. Hall and Y. Luo at UNB for their assistance with the SEM, microprobe, and LA ICP-MS analyses. Primary funding for this project was provided by the Northwest Territories Geoscience Office (NTGO Contribution Number 73), and the Natural Sciences and Engineering Research Council of Canada (NSERC CGS-M). Additional support was provided by MAC, MPDA, SEG, International Lithium Corp. and Aurora Geosciences Ltd.

Electronic supplementary material. The complete tables of columbite–tantalite phases (S1) and muscovite mineral chemistry (S2) as well as a comparison of trace-element contents in muscovite throughout the pegmatite field (S3) are available online at the Journal web site *(http://dx.doi.org/10.3190/jgeosci.149)*.

References

Anderson MO (2013) Evolution and Mineralization of the Moose II Lithium–Tantalum Pegmatite Deposit, Northwest Territories, Canada. Unpublished M.Sc. thesis, University of New Brunswick, Fredericton, pp 1–335

Ayres L, Černý P (1982) Metallogeny of granitoid rocks in the Canadian Shield. Canad Mineral 20: 439–539

Bartels A, Holtz F, Linnen RL (2010) Solubility of manganotantalite and manganocolumbite in pegmatitic melts. Amer Miner 95: 537–544

Bleeker W, Davis WJ (1999) The 1991–1999 NATMAP Slave Province project: introduction. Can J Earth Sci 36: 1033–1042

Bleeker W, Hall B (2007) The Slave Craton: geologic and metallogenic evolution. In: Goodfellow WD (ed) Mineral Deposits of Canada: a Synthesis of Major Deposit-Types, District Metallogeny, the Evolution of Geological Provinces, and Exploration Methods. Geological Association of Canada, Mineral Deposits Division, St. John's, NFLD, Canada, pp 849–879

Bleeker W, Ketchum JWF, Davis WJ, Villeneuve ME (1999) The Central Slave Basement Complex: Part I: its structural topology and autochthonous cover. Can J Earth Sci 36: 1083–1109

Chevychelov VY, Zaraisky GP, Borisovsky SE (1998) Solubility of columbite–tantalite in the melts of Li–F granite, and pegmatite–aplite banded rocks from the Orlovka tantalum deposit in eastern Transbaikalia. Exper Geo 7: 9–11

Chevychelov VY, Zaraisky GP, Borisovsky SE, Borkov DA (2004) Partitioning of Ta and Nb between magmatic melt and aqueous (K,Na,H)F-containing fluid: effects of temperature and chemical composition of the melt. EMPG-X Symposium Abstracts, Frankfurt, Germany, Lithos supplement to vol 73(1–2), pp S17

Chevychelov, VY, Zaraisky GP, Borisovsky SE, Borkov DA (2005) Effect of melt composition and temperature on the partitioning of Ta, Nb, Mn and F between granitic (alkaline) melt and fluorine-bearing aqueous fluid: fractionation of Ta and Nb and conditions of ore formation in rare-metal granites. Petrologiya 13: 339–357

Chevychelov VY, Borodulin GP, Zaraisky GP (2010) Solubility of columbite, $(Mn,Fe)(Nb,Ta)_2O_6$, in granitoid and alkaline melts at 650–850 °C: an experimental investigation. Geochem Int 48: 456–464

Chudík P, Uher P, Gadas P, Škoda R, Pršek J (2011) Niobium–tantalum oxide minerals in the Jezuitské Lesy granitic pegmatite, Bratislava Massif, Slovakia: Ta to

Nb and Fe to Mn evolutionary trends in a narrow, Be, Cs-rich and Li, B-poor dike. Eur J Mineral 102: 55–27

Černý P (2005) The Tanco rare-element pegmatite deposit, Manitoba: regional context, internal anatomy, and global comparisons. In: Linnen RL, Samson IM (eds) Rare-Element Geochemistry of Ore Deposits. Geological Association of Canada Short Course Notes 17: pp 127–158

Černý P, Ercit TS (1985) Some recent advances in the mineralogy and geochemistry of Nb and Ta in rare-element granitic pegmatites. Bull Minéral 108: 499–532

Černý P, Meintzer RE, Anderson AJ (1985) Extreme fractionation in rare-element granitic pegmatites: selected examples of data and mechanisms. Canad Mineral 23: 381–421

Černý P, Goad BE, Hawthorne FC, Chapman R (1986) Fractionation trends of the Nb- and Ta-bearing oxide minerals in the Greer Lake pegmatitic granite and its pegmatite aureole, southeastern Manitoba. Amer Miner 71: 501–517

Černý P, Ercit TS, Wise MA (1992) The tantalite–tapiolite gap: natural assemblages versus experimental data. Canad Mineral 30: 587–596

Davis WJ, Bleeker W (1999) Timing of plutonism, deformation, and metamorphism in the Yellowknife Domain, Slave Province, Canada. Can J Earth Sci 36: 1169–1187

Ercit TS, Wise MA, Černý P (1995) Compositional and structural systematics of the columbite group. Amer Miner 80: 613–619

Henderson JB (1981) Archean basin evolution in the Slave Province, Canada. In: Kröner A (ed) Plate Tectonics in the Precambrian. Developments in Precambrian Geology 4. Elsevier, Amsterdam, pp 213–235

Henderson JB (1987) Burwash Formation at Yellowknife, NWT. In: Padgham WA (ed) Field Guide, Yellowknife '87, Summer Field Meeting. Geological Association of Canada, Yellowknife, pp 21–32

Keppler H (1993) Influence of fluorine on the enrichment of high field strength trace elements in granitic rocks. Contrib Mineral Petrol 114: 479–488

King J, Helmstaedt H (1997) The Slave Province, Northwest Territories, Canada. In: de Wit MJ, Ashwal LD (eds) Greenstone Belts. Oxford Monographs on Geology and Geophysics, USA, pp 459–479

Kontak DJ (2006) Nature and origin of an LCT-suite pegmatite with late-stage sodium enrichment, Brazil Lake, Yarmouth County, Nova Scotia. I. Geological setting and petrology. Canad Mineral 44: 563–598

Lahti SI (1987) Zoning in columbite–tantalite crystals from the granitic pegmatites of the Erajarvi area, southern Finland. Geochim Cosmochim Acta 51: 509–517

Linnen RL (1998) The solubility of Nb–Ta–Zr–Hf in granitic melts with Li and Li + F: constraints for mineralization in rare metal granites and pegmatites. Econ Geol 93: 1013–1025

Linnen RL, Cuney M (2005) Granite-related rare-element deposits and experimental constraints on Ta–Nb–W–Sn–Zr–Hf mineralization. In: Linnen RL, Sampson IM (eds) Rare-Element Geochemistry and Mineral Deposits. Geological Association of Canada, Short Course Notes 17: pp 45–68

Linnen RL, Keppler H (1997) Columbite solubility in granitic melts: consequences for the enrichment and fractionation of Nb and Ta in the Earth's crust. Contrib Mineral Petrol 128: 213–227

Linnen RL, Van Lichtervelde M, Černý P (2012) Granitic pegmatites as sources of strategic metals. Elements 8: 275–280

London D (1987) Internal differentiation of rare-element pegmatites: effects of boron, phosphorous, and fluorine. Geochim Cosmochim Acta 51: 403–420

London D (1990) Internal differentiation of rare-element pegmatites: a synthesis of recent research. In: Stein HL, Hannah JL (eds) Ore-Bearing Granitic Systems: Petrogenesis and Mineralizing Processes. Geological Society of America, Boulder, CO, pp 35–50

London D (2005) Geochemistry of alkalies and alkaline earths in ore-forming granites, pegmatites, and rhyolites. In: Linnen RL, Samson IM (eds) Rare-Element Geochemistry of Ore Deposits. Geological Association of Canada, Short Course Notes 17: pp 17–43

London D (2008) Pegmatites. The Mineralogical Association of Canada, Québec, QC, pp 1–347

London D, Morgan GB (2004) Alkali fractionation and feldspar zonation in granitic pegmatites. Geological Society of America Abstracts with Programs 36: 46

Meintzer RE (1987) The Mineralogy and Geochemistry of Granitoid Rocks and Related Pegmatites of the Yellowknife Pegmatite Field, Northwest Territories. Unpublished Ph.D. thesis, University of Manitoba, Winnipeg, pp 1–1642

Monier G, Robert, JL (1986) Muscovite solid solutions in the system K_2O–MgO–FeO–Al_2O_3–SiO_2–H_2O: an experimental study at 2 kbar P_{H2O} and comparison with natural Li-free white mica. Mineral Mag 50: 257–266

Novák M, Černý P, Uher P (2003) Extreme variation and apparent reversal of Nb–Ta fractionation in columbite-group minerals from Scheibengraben beryl–columbite granitic pegmatite, Maršíkov, Czech Republic. Eur J Mineral 15: 565–574

Ootes L, Davis WJ, Bleeker W, Jackson VA (2009) Two distinct ages of Neoarchean turbidites in the western Slave Craton: further evidence and implications for a possible back-arc model. J Geol 117: 15–36

Padgham WA, Fyson WK (1992) The Slave Province: a distinct Archean Craton. Can J Earth Sci 29: 2072–2086

Putnis A, Fernandez DL, Prieto M (1992) Experimentally produced oscillatory zoning in the (Ba,Sr)SO_4 solid solution. Nature 358: 743–745

Tindle AG (2001a) Chemical formula recalculation for columbite–tantalite & ferrotapiolite analyses. Accessed January 13, 2013 at *http://www.open.ac.uk/earth-research/tindle/AGTWebData/Mica-musc.xls*

Tindle AG (2001b) Muscovite formula unit calculations – with optional calculated Li_2O. Accessed November 20, 2012 at *http://tabitha.open.ac.uk/tindle/AGTHome.html*

Tindle AG, Breaks FW (2000) Columbite–tantalite mineral chemistry from rare-element granitic pegmatites: Separation Lake area, N.W. Ontario, Canada. Mineral Petrol 70: 165–198

Tindle AG, Webb PC (1990) Estimation of lithium contents in trioctahedral micas using microprobe data: application to micas from granitic rocks. Eur J Mineral 2: 595–610

Van Lichtervelde M, Salvi S, Béziat D, Linnen RL (2007) Textural features and chemical evolution in tantalum oxides: magmatic versus hydrothermal origins for Ta mineralization in the Tanco lower pegmatite, Manitoba, Canada. Econ Geol 102: 257–276

Van Lichtervelde M, Grégoire M, Linnen RL, Béziat D, Salvi S (2008) Trace element geochemistry by Laser Ablation ICP-MS of micas associated with Ta mineralization in the Tanco pegmatite, Manitoba, Canada. Contrib Mineral Petrol 155: 791–806

Veksler IV, Thomas R (2002) An experimental study of B-, P- and F-rich synthetic granitic pegmatite at 0.1 and 0.2 GPa. Contrib Mineral Petrol 143: 673–683

Wedepohl KH (1995) The composition of the continental crust. Geochim Cosmochim Acta 59: 1217–1232

Whitney DL, Evans BW (2010) Abbreviations for names of rock-forming minerals. Amer Miner 95: 185–187

Wise MA (1987) Geochemistry and crystal chemistry of Nb, Ta, and Sn minerals from the Yellowknife pegmatite field, NWT. Unpublished M.Sc. thesis, University of Manitoba, Winnipeg, pp 1–712

Wood SA, Williams-Jones AE (1993) Theoretical studies of the alteration of spodumene, petalite, eucryptite and pollucite in granitic pegmatites: exchange reactions with alkali feldspars. Contrib Mineral Petrol 114: 255–263

Zaraisky GP, Korzhinskaya V, Kotova N (2010) Experimental studies of Ta_2O_5 and columbite–tantalite solubility in fluoride solutions from 300 to 550 °C and 50 to 100 MPa. Mineral Petrol 99: 287–300